Design of an Atmospheric Model Based on a Generalized Vertical Coordinate

CELAL S. KONOR AND AKIO ARAKAWA

Department of Atmospheric Sciences, University of California, Los Angeles, Los Angeles, California

(Manuscript received 1 May 1996, in final form 7 October 1996)

ABSTRACT

Although there are important advantages in the use of an isentropic vertical coordinate in atmospheric models, it requires overcoming computational difficulties associated with intersections of coordinate surfaces with the earth's surface. In this paper, the authors present a model based on the generalized vertical coordinate, $\zeta = F(\theta, p, p_S)$, in which an isentropic coordinate can be combined with a terrain-following σ coordinate near the surface with a smooth transition between the two. One of the key issues in developing such a model is to satisfy consistency between the predictions of the pressure and the potential temperature. In the model presented in this paper, consistency is maintained by the use of an equation that determines the vertical mass flux. A procedure to properly choose $\zeta = F(\theta, p, p_S)$ is also presented, which guarantees that ζ is a monotonic function of height even when unstable stratification occurs.

In the vertical discretization, the Charney–Phillips grid is used since, with this grid, it is straightforward to satisfy the thermodynamic equation when $\zeta = \theta$. In the generalized vertical coordinate, determining the pressure gradient force requires both the Montgomery potential and the geopotential at the same levels. The discrete hydrostatic equation is designed to maintain consistency between the two. The vertically discrete equations also satisfy two important integral constraints. With these features, the model becomes identical to the isentropic coordinate model developed by Hsu and Arakawa when $\zeta = \theta$.

To demonstrate the performance of the model, the simulated nonlinear evolution of a midlatitude disturbance starting from random disturbances is presented. In the simulation, physical processes are represented by simple thermal forcing in the form of Newtonian heating and friction in the form of Rayleigh damping. During the evolution of the disturbance, the model generates sharp fronts both at the surface and in the upper and middle troposphere. No serious computational difficulties are found in this simulation.

1. Introduction

The basic vertical coordinates being used in atmospheric models are the height z, the pressure p, the normalized pressure $\sigma \equiv p/p_S$, and the potential temperature $\theta \equiv T(p_0/p)^{\kappa}$, where p_S is the surface pressure, T is the temperature, p_0 is a standard pressure, $\kappa \equiv R/c_p$, R is the gas constant, and c_p is the specific heat at constant pressure. The majority of models based on the primitive equations use the σ coordinate or its variations such as those used by Arakawa and Lamb (1977) and Simmons and Burridge (1981). With this coordinate, the earth's surface is a coordinate surface and, therefore, the lower boundary condition reduces to $\dot{\sigma} \equiv D\sigma/Dt = 0$. The expense we pay for this simplification is the complication of the pressure gradient force, which becomes $-(\nabla_p \Phi) \equiv -\nabla_\sigma \Phi - (RT/p_S)\nabla p_S$, where Φ is the geopotential. The two terms on the right-hand side of this expression have comparable magnitudes with opposite sign over steep topography and thus their sum may be subject to large errors. Moreover, coordinate surfaces in the σ coordinate can be very different from surfaces of actual motion. This generally leads to larger discretization errors for advection processes.

There are important advantages in the use of an isentropic vertical coordinate (θ coordinate) at least away from the surface. Since isentropic surfaces are material surfaces under adiabatic processes, discretization errors for vertical advection are virtually eliminated with this coordinate. Consequently, the use of the θ coordinate is advantageous for accurate simulations of condensation processes since the transport of moisture takes place along isentropic surfaces prior to the onset of condensation (see Johnson et al. 1993). Moreover, the pressure gradient force is expressed as $-\nabla_\theta M$ with the θ coordinate, which is an irrotational vector when the curl is taken along a coordinate surface. Here M is the Montgomery potential given by $M \equiv c_p T + \Phi$. Consequently, Ertel's potential vorticity for the quasi-static system can be expressed in the most straightforward way as $(\zeta_\theta + f)(-\partial p/\partial\theta)^{-1}$, where $\zeta_\theta \equiv \mathbf{k}\cdot\nabla_\theta \times \mathbf{v}$, $\mathbf{k}$ is the vertical unit vector, $\mathbf{v}$ is the horizontal velocity, f is the Coriolis parameter $2\Omega \sin\varphi$, Ω is the earth's angular velocity, and φ is the latitude.

There are, however, computational difficulties to be

Corresponding author address: Dr. Celal S. Konor, Department of Atmospheric Sciences, University of California, Los Angeles, 405 Hilgard Avenue, Los Angeles, CA 90095-1565.
E-mail: csk@uygar.atmos.ucla.edu

overcome in constructing an isentropic coordinate model, the most challenging of which are associated with the intersections of coordinate surfaces with the earth's surface. An approach to deal with the intersections is introduced by Eliassen and Raustein (1968). Their model consists of two isentropic layers, one of which intersects the earth's surface. The mass and the horizontal velocity are predicted for each model layer. In addition, the potential temperature is predicted at the earth's surface using the thermodynamic equation, in which the derivatives are obtained by extrapolating the intersecting isentropic surfaces into the ground. Multilayer versions of the same model were later constructed by Eliassen and Raustein (1970) and Shapiro (1974, 1975). Bleck (1973, 1977) also followed this approach. Bleck (1984), however, introduced a different approach through which intersecting isentropic surfaces are extended along the earth's surface introducing ''massless layers.'' With this approach the potential temperature at the earth's surface is not directly predicted using the thermodynamic equation; instead the positions of intersecting isentropic surfaces are determined as the edges of the ''massless layers'' predicted by the continuity equation applied to isentropic layers.

The massless layer approach is also used in the model developed by Hsu and Arakawa (1990), which was used to simulate the nonlinear evolution of extratropical cyclones and associated frontogenesis (see also Arakawa et al. 1992). These simulations demonstrated the model's ability to generate and maintain sharp fronts in the upper and middle troposphere without serious computational difficulties. The performance of the model, however, is relatively poor near the surface. Analyses of the simulated fields indicate that the poor performance is due to the determination of the surface (potential) temperature at grid points from a relatively limited number of intersecting isentropic surfaces.

Another approach to eliminate the difficulties associated with isentropic surfaces intersecting with the earth's surface is to couple a σ-coordinate domain near the surface with an isentropic coordinate domain above. In a model following this approach, a set of internal boundary conditions is used at the interface of the two domains to match the solutions. Deaven's (1976) two-dimensional model, for example, treated the interface as a material surface, which was initially placed at 700 mb. Friend et al. (1977), on the other hand, placed the interface at a constant pressure surface by allowing mass flux across it. Gall and Johnson (1977) also treated the interface as a material surface at a fixed height. Uccellini et al. (1979), Johnson and Uccellini (1983) and Black (1984) constructed their models basically following Gall and Johnson (1977) but placing the interface at a constant sigma surface allowing mass flux across it. Bleck (1978a), on the other hand, proposed putting the interface at a sufficiently high isentropic surface that does not intersect the earth's surface. While this eliminates the computational problems associated with intersecting isentropic surfaces, it loses the advantage of using the isentropic coordinate in the lower troposphere.

Hybrid coordinate models of the type discussed above are still being used. In later versions of the hybrid σ–θ model of Johnson and Uccellini (Zapotocny et al. 1994), the matching conditions at the interface of the sigma and isentropic domains are considerably improved. Despite the improvements, these models still remain susceptible to the computational problems caused by the intersection of isentropic surfaces with the interface.

The latest approach is based on the use of a generalized vertical coordinate (Bleck 1978b, 1979), in which two or more coordinates are combined to define a single coordinate. An example of this approach is the hybrid σ–θ–p coordinate used in the model by Zhu et al. (1992). The coordinate is a generalization of Simmons and Burridge's (1983) hybrid σ–p coordinate by including a θ domain between the σ domain near the surface and the p domain near the upper boundary. Another example of the generalized vertical coordinate approach is Bleck and Benjamin's (1993) hybrid σ–θ coordinate. A model based on this vertical coordinate is currently in service to perform short-term regional weather predictions to support a mesoscale analysis and prediction system (MAPS) at NOAA/FSL.

It is important to remember that, to determine the thermal structure with the p or σ coordinate, θ is predicted while p is predicted for that purpose with the θ coordinate. Therefore, with a generalized vertical coordinate that has smooth transitions between its σ domain and θ domain, both p and θ must be predicted. This generally introduces redundancy unless the predictions are consistent with each other. There are also problems in designing the discrete hydrostatic equation since, with the p or σ coordinate, the hydrostatic equation is used to determine the difference of the geopotential from two adjacent levels while, with the θ coordinate, it is used to determine the difference of the Montgomery potential between those levels.

Keeping these problems in mind, we developed our own model based on a generalized vertical coordinate. The vertical coordinate is defined as $\zeta \equiv F(\theta, p, p_S)$, where F is a monotonic function of height, allowing any hybrid combination of p, σ, and θ. A staggered Charney–Phillips grid (CP-grid, see Arakawa and Konor 1996) is used for the vertical discretization, in which both the potential temperature and pressure are predicted at the same coordinate surfaces. The consistency between the predictions of pressure and potential temperature is guaranteed through the use of an equation that determines the vertical mass flux. When $\zeta \equiv \theta$, the model becomes identical to the isentropic coordinate model developed by Hsu and Arakawa (1990).

Section 2 reviews the basic governing equations in a generalized vertical coordinate and some of their integral properties for the continuous case. Section 2 also derives the continuous version of the vertical mass flux

equation that guarantees consistency mentioned above. A method to choose F in $\zeta \equiv F(\theta, p, p_S)$ is also described. In section 3, we discuss the vertical grid and vertically discrete equations, including the vertically discrete version of the vertical mass flux equation. The discrete equations derived in section 3 are summarized in appendix A. The horizontal and time discretizations are described in section 4, with a summary in appendix B. In section 5, additional features of the model are discussed. These features include vertical momentum diffusion to control the artificial velocities in the layers with small mass. The nonlinear evolution of a midlatitude disturbance simulated using the model is presented in section 6. Finally, conclusions and a summary are presented in section 7.

2. Equations with a generalized vertical coordinate in their continuous forms

In this section, we present the continuous system of equations in a generalized vertical coordinate. Section 2c derives the vertical mass flux equation in its continuous form. Section 2e presents a method to choose F in $\zeta \equiv F(\theta, p, p_S)$ through which ζ is guaranteed to be monotonic in height.

a. Basic governing equations in a generalized coordinate

In this section, we present the basic governing equations using a generalized vertical coordinate (ζ coordinate). With this coordinate, the material time derivative is expressed as

$$\frac{D}{Dt} \equiv \left(\frac{\partial}{\partial t}\right)_\zeta + \mathbf{v}\cdot\boldsymbol{\nabla}_\zeta + \dot{\zeta}\frac{\partial}{\partial \zeta}, \tag{2.1}$$

where $\dot{\zeta} \equiv D\zeta/Dt$. The vertical p-velocity ω, for example, can be expressed as

$$\omega \equiv \frac{Dp}{Dt} = \left(\frac{\partial p}{\partial t}\right)_\zeta + \mathbf{v}\cdot\boldsymbol{\nabla}_\zeta p - m\dot{\zeta}, \tag{2.2}$$

where

$$m \equiv -\frac{\partial p}{\partial \zeta}. \tag{2.3}$$

When ζ is an increasing function of height, mg^{-1} is the mass per unit increment of ζ per unit horizontal area.

Using m, the hydrostatic equation can be written as

$$\frac{\partial \Phi}{\partial \zeta} = \alpha m, \tag{2.4}$$

where α is the specific volume. Also using m, the continuity equation can be written as

$$\left(\frac{\partial m}{\partial t}\right)_\zeta + \boldsymbol{\nabla}_\zeta\cdot(m\mathbf{v}) + \frac{\partial}{\partial \zeta}(m\dot{\zeta}) = 0. \tag{2.5}$$

If the boundaries in the vertical are material surfaces, we have

$$(m\dot{\zeta}) = 0 \quad \text{at} \quad \zeta = \zeta_T, \zeta_S, \tag{2.6}$$

where the subscripts T and S denote the upper and lower boundaries, respectively. We assume ζ_T and ζ_S are constants so that the boundaries are coordinate surfaces.

The model atmosphere is assumed to be a perfect gas so that the equation of state is given by

$$\alpha = \frac{RT}{p}. \tag{2.7}$$

We express the potential temperature as

$$\theta = \frac{c_p T}{\Pi}, \tag{2.8}$$

where Π is the Exner function defined by

$$\Pi \equiv c_p\left(\frac{p}{p_0}\right)^\kappa. \tag{2.9}$$

The thermodynamic equation is given by

$$c_p\frac{DT}{Dt} = c_p\left[\left(\frac{\partial T}{\partial t}\right)_\zeta + \mathbf{v}\cdot\boldsymbol{\nabla}_\zeta T + \dot{\zeta}\frac{\partial T}{\partial \zeta}\right] = \alpha\omega + Q, \tag{2.10}$$

where Q is the heating per unit mass. Using the potential temperature θ, the thermodynamic equation can also be written as

$$\frac{D\theta}{Dt} = \left(\frac{\partial \theta}{\partial t}\right)_\zeta + \mathbf{v}\cdot\boldsymbol{\nabla}_\zeta\theta + \dot{\zeta}\frac{\partial \theta}{\partial \zeta} = \frac{Q}{\Pi}. \tag{2.11}$$

The momentum equation can be written as

$$\begin{aligned}\frac{D\mathbf{v}}{Dt} &= \left(\frac{\partial \mathbf{v}}{\partial t}\right)_\zeta + \mathbf{v}\cdot\boldsymbol{\nabla}_\zeta\mathbf{v} + \dot{\zeta}\frac{\partial \mathbf{v}}{\partial \zeta} \\ &= -(\boldsymbol{\nabla}_p\Phi) - f\mathbf{k}\times\mathbf{v} + \mathbf{F},\end{aligned} \tag{2.12}$$

where $\mathbf{F}$ is the friction force. Using the relation

$$\boldsymbol{\nabla}_p = \boldsymbol{\nabla}_\zeta - \boldsymbol{\nabla}_\zeta p\frac{\partial}{\partial p} \tag{2.13}$$

and (2.3), the horizontal pressure gradient force can be written as

$$-\boldsymbol{\nabla}_p\Phi = -\boldsymbol{\nabla}_\zeta\Phi - \frac{1}{m}\frac{\partial \Phi}{\partial \zeta}\boldsymbol{\nabla}_\zeta p. \tag{2.14}$$

Using the Montgomery potential $M \equiv c_pT + \Phi$, (2.4), (2.7), (2.8), and (2.9) in (2.14), we may rewrite (2.14) as

$$-\boldsymbol{\nabla}_p\Phi = -\boldsymbol{\nabla}_\zeta M + \Pi\boldsymbol{\nabla}_\zeta\theta. \tag{2.15}$$

When $\zeta \equiv \theta$, the right-hand side of (2.15) reduces to $-\boldsymbol{\nabla}_\theta M$. Maintaining this is one of the essential features in our model.

Substituting (2.3) into the first term in (2.5), inte-

grating with respect to ζ from ζ_T to ζ, and using (2.6), we obtain the pressure tendency equation,

$$\left(\frac{\partial p}{\partial t}\right)_\zeta = \frac{\partial p_T}{\partial t} + \nabla_\zeta \cdot \int_{\zeta_T}^{\zeta} m\mathbf{v}\, d\zeta + (m\dot{\zeta})_\zeta. \quad (2.16)$$

Applying (2.16) to $\zeta = \zeta_S$ and using (2.6), we obtain the surface pressure tendency equation,

$$\frac{\partial p_S}{\partial t} = \frac{\partial p_T}{\partial t} + \nabla \cdot \int_{\zeta_T}^{\zeta_S} m\mathbf{v}\, d\zeta. \quad (2.17)$$

b. *Expressing integral constraints with the generalized ζ coordinate*

In this section, we express a set of integral constraints used in the generalized ζ-coordinate model. The first two of the four constraints used by Arakawa and Lamb (1977) in designing a vertical difference scheme are 1) vertically integrated pressure gradient force generates no circulation along a contour of the surface topography and 2) the energy conversion terms in the thermodynamic and kinetic energy equations have the same form with opposite sign so that the total energy is conserved under adiabatic frictionless conditions.

1) VERTICALLY INTEGRATED HORIZONTAL PRESSURE GRADIENT FORCE

The horizontal pressure gradient force (2.14) can be rewritten as

$$-(\nabla_p \Phi) = -\frac{1}{m}\nabla_\zeta(m\Phi) - \frac{1}{m}\frac{\partial}{\partial\zeta}(\Phi\nabla_\zeta p). \quad (2.18)$$

Here (2.3) has been used. The vertical mass integral of (2.18) is

$$-\int_{\zeta_T}^{\zeta_S} m\nabla_p\Phi\, d\zeta = -\nabla_\zeta \int_{\zeta_T}^{\zeta_S} (m\Phi)\, d\zeta - \Phi_S\nabla p_S + \Phi_T\nabla p_T. \quad (2.19)$$

If $\nabla p_T = 0$, the right-hand side vanishes when (2.19) is integrated along a contour of the surface of topography on which Φ_S is constant so that constraint 1 is satisfied.

2) CONSERVATION OF THE TOTAL ENERGY

Multiplying the momentum equation (2.12) with (2.14) by $m\mathbf{v}$ and using (2.2), (2.3), (2.4), (2.5), and (2.18), we obtain the kinetic energy equation

$$\left(\frac{\partial}{\partial t}\right)_\zeta\left(m\frac{\mathbf{v}^2}{2}\right) + \nabla_\zeta\cdot\left(m\frac{\mathbf{v}^2}{2}\mathbf{v}\right) + \frac{\partial}{\partial\zeta}\left(m\frac{\mathbf{v}^2}{2}\dot{\zeta}\right) = -\nabla_\zeta\cdot(m\Phi\mathbf{v}) + \frac{\partial}{\partial\zeta}\left[\Phi\left(\frac{\partial p}{\partial t} - m\dot{\zeta}\right)\right] - m\alpha\omega + m\mathbf{v}\cdot\mathbf{F}. \quad (2.20)$$

The first and second terms on the right-hand side of (2.20) represent the convergence of horizontal and vertical energy fluxes that involve Φ. The term $m\alpha\omega$, on the other hand, represents the energy conversion from potential energy to kinetic energy. Using (2.5) and (2.10), the thermodynamic energy equation can be written in flux form as

$$\left(\frac{\partial}{\partial t}\right)_\zeta(mc_pT) + \nabla_\zeta\cdot(mc_pT\mathbf{v}) + \frac{\partial}{\partial\zeta}(mc_pT\dot{\zeta}) = m(\alpha\omega + Q). \quad (2.21)$$

If $\partial p_T/\partial t = 0$, all terms vanish under adiabatic frictionless conditions when the sum of (2.20), (2.21), and $\partial(\Phi_S p_S)/\partial t = \Phi_S(\partial p_S/\partial t)$ is integrated over the entire atmosphere, so that constraint 2 is satisfied.

c. *The vertical mass flux equation*

In this section we derive the vertical mass flux equation, which is one of the key features of the model described in this paper. Let us define the generalized ζ coordinate by

$$\zeta \equiv F(\theta, p, p_S). \quad (2.22)$$

It is assumed that ζ varies monotonically with height (see section 2e). When $F \equiv \theta$, the coordinate reduces to the θ coordinate. When $F \equiv p$, the coordinate reduces to the p coordinate. When $F \equiv p/p_S$, the coordinate reduces to the σ coordinate proposed by Phillips (1957). When $F \equiv p/p_S + (p/p_S - 1)(p/p_S - p/p_C)$, on the other hand, where p_C is a constant pressure, the coordinate reduces to the hybrid σ–p coordinate of Simmons and Burridge (1981).

In a model based on the ζ coordinate, ζ remains unchanged on each coordinate surface. In the form given by (2.22), however, all of the three variables (θ, p, and p_S) are predicted. If these predictions are done independently, F on a coordinate surface generally changes in time. Consequently, even when F varies monotonically with height, the variation of ζ with height may not be monotonic so that crossing of coordinate surfaces may occur. This situation, however, can be eliminated by requiring

$$0 = \left(\frac{\partial}{\partial t}\right)_\zeta F(\theta, p, p_S), \quad (2.23)$$

which is obtained by differentiating (2.22) with respect to t under constant ζ.

From (2.23), we can derive a diagnostic relationship that determines the vertical mass flux $m\dot{\zeta}$. First, using (2.22) in (2.23),

$$\left(\frac{\partial F}{\partial\theta}\right)_{p,p_S}\left(\frac{\partial\theta}{\partial t}\right)_\zeta + \left(\frac{\partial F}{\partial p}\right)_{\theta,p_S}\left(\frac{\partial p}{\partial t}\right)_\zeta + \left(\frac{\partial F}{\partial p_S}\right)_{\theta,p}\frac{\partial p_S}{\partial t} = 0. \quad (2.24)$$

Substituting (2.11), (2.16), and (2.17) in (2.24), we obtain

$$\left\{\left(\frac{\partial F}{\partial \theta}\right)_{p,p_S}\left(\frac{\partial \theta}{\partial \zeta}\right) - m\left(\frac{\partial F}{\partial p}\right)_{\theta,p_S}\right\}\dot{\zeta}$$
$$= \left(\frac{\partial F}{\partial \theta}\right)_{p,p_S}\left\{\frac{Q}{\Pi} - \mathbf{v}\cdot\boldsymbol{\nabla}_\zeta\theta\right\}$$
$$+ \left(\frac{\partial F}{\partial p}\right)_{\theta,p_S}\left\{\frac{\partial p_T}{\partial t} + \boldsymbol{\nabla}_\zeta\cdot\int_{\zeta_T}^{\zeta} m\mathbf{v}\, d\zeta\right\}$$
$$+ \left(\frac{\partial F}{\partial p_S}\right)_{\theta,p}\left\{\frac{\partial p_T}{\partial t} + \boldsymbol{\nabla}\cdot\int_{\zeta_T}^{\zeta_S} m\mathbf{v}\, d\zeta\right\}. \quad (2.25)$$

We call (2.25) the (generalized) vertical mass flux equation. When $F \equiv p$ and $\partial p_T/\partial t = 0$, for which m is a constant and $\dot{\zeta} = \omega$, (2.25) gives

$$\omega = -\int_{p_T}^{p} \boldsymbol{\nabla}_p\cdot\mathbf{v}\, dp, \quad (2.26)$$

which can be readily obtained from $\partial\omega/\partial p + \boldsymbol{\nabla}_p\cdot\mathbf{v} = 0$ for the pressure coordinate. When $F \equiv \sigma = (p - p_T)(p_S - p_T)^{-1}$ and $\partial p_T/\partial t = 0$, for which $(\partial F/\partial p_S)_{\theta,p} = -\sigma(\partial F/\partial p)_{\theta,p_S}$, $m \equiv p_S - p_T$ and $\dot{\zeta} = \dot{\sigma}$, (2.24) gives

$$-(m\dot{\sigma}) = \boldsymbol{\nabla}_\sigma\cdot\int_{\sigma_T}^{\sigma} m\mathbf{v}\, d\sigma - \sigma\boldsymbol{\nabla}\cdot\int_{\sigma_T}^{\sigma_S} m\mathbf{v}\, d\sigma. \quad (2.27)$$

Equation (2.27) is identical to the vertical mass flux equation for the σ coordinate (see Arakawa and Lamb 1977; Simmons and Burridge 1981; Arakawa and Suarez 1983). When $F \equiv \theta$, on the other hand, for which $\dot{\zeta} = \dot{\theta} \equiv (D\theta/Dt)$, (2.24) gives

$$\dot{\theta} = \frac{Q}{\Pi}. \quad (2.28)$$

This is the first law of thermodynamics used to determine the vertical mass flux in a model based on the θ coordinate.

d. Conditions at the upper boundary

Equation (2.23) is also required at the upper boundary so that

$$0 = \left(\frac{\partial}{\partial t}\right)_\zeta F(\theta_T, p_T, p_S). \quad (2.29)$$

From (2.29), similarly to (2.24), we obtain

$$\left(\frac{\partial F}{\partial \theta_T}\right)_{p_T,p_S}\left(\frac{\partial \theta_T}{\partial t}\right)_\zeta + \left(\frac{\partial F}{\partial p_T}\right)_{\theta_T,p_S}\left(\frac{\partial p_T}{\partial t}\right)_\zeta + \left(\frac{\partial F}{\partial p_S}\right)_{\theta_T,p_T}\frac{\partial p_S}{\partial t} = 0. \quad (2.30)$$

When $(\partial p_T/\partial t)_\zeta = 0$ is assumed and F is chosen such a way that $(\partial F/\partial p_S)_{\theta_T,p_T} = 0$, (2.30) becomes

$$\left(\frac{\partial F}{\partial \theta_T}\right)_{p_T,p_S}\left(\frac{\partial \theta_T}{\partial t}\right)_\zeta = 0. \quad (2.31)$$

If $F \equiv p$ at the upper boundary, $(\partial F/\partial\theta_T)_{p_T,p_S} = 0$ so that (2.31) is trivially satisfied. If $F \equiv \theta$ at the upper boundary, on the other hand, (2.31) requires $(\partial\theta_T/\partial t)_\zeta \equiv 0$. This is a consequence of our assumption that the upper boundary is a coordinate surface.

e. Choices for $\zeta = F(\theta, p, p_S)$

The generalized vertical coordinate $\zeta = F(\theta, p, p_S)$ can be used as the p coordinate, the σ coordinate, the θ coordinate, or any combination of them provided that ζ changes monotonically with height and is constant at the top and bottom boundaries.

Our own purpose for using this coordinate is to combine the advantages of the isentropic coordinate away from the surface with the advantages of the standard σ coordinate near the surface. If we define $\sigma \equiv \sigma(p, p_S)$ as a monotonically *increasing* function of height, a hybrid σ–θ vertical coordinate may be required to satisfy

$$\frac{\partial\zeta}{\partial\sigma} > 0 \quad (2.32)$$

and

$$\zeta = \begin{cases} \text{const}, & \sigma = \sigma_S \\ \theta, & \sigma = \sigma_T \end{cases}, \quad (2.33)$$

where σ_S and σ_T are constants. The requirements (2.33) can be satisfied by

$$\zeta \equiv f(\sigma) + g(\sigma)\theta \quad (2.34)$$

with

$$\left.\begin{array}{ll} g(\sigma) \to 0; & \sigma \to \sigma_S \\ f(\sigma) \to 0, \quad g(\sigma) \to 1; & \sigma \to \sigma_T \end{array}\right\}. \quad (2.35)$$

With (2.34), (2.32) can be satisfied if

$$\frac{df}{d\sigma} + \frac{dg}{d\sigma}\theta + g\frac{\partial\theta}{\partial\sigma} > 0. \quad (2.36)$$

Any pair of $f(\sigma)$ and $g(\sigma)$ that satisfy (2.35) and (2.36) can be used in (2.34) to define the hybrid σ–θ vertical coordinate. To simplify the selection process, here we present an analytical method in which $f(\sigma)$ can be chosen for a prescribed $g(\sigma)$.

Let us require that $g(\sigma)$ be a monotonically increasing function of height between σ_S and σ_T, and define $\theta_{\min}$ and $(\partial\theta/\partial\sigma)_{\min}$ as properly chosen lower bounds of the potential temperature and static stability, respectively. [Note that $(\partial\theta/\partial\sigma)_{\min}$ is positive when stable according to our choice of σ.] Then, (2.36) can be satisfied if we choose $f(\sigma)$ from

$$\frac{df}{d\sigma} + \frac{dg}{d\sigma}\theta_{\min} + g\left(\frac{\partial\theta}{\partial\sigma}\right)_{\min} = 0. \quad (2.37)$$

In (2.37), $\theta_{\min}$ and $(\partial\theta/\partial\sigma)_{\min}$ can be either functions of height or constants. After a proper choice is made for $g(\sigma)$ that satisfies (2.35), (2.37) with (2.35) can be solved to obtain $f(\sigma)$. Then ζ can be obtained by using $f(\sigma)$ and $g(\sigma)$ in (2.32). In this way, unstable stratifications ($\partial\theta/\partial z < 0$) may occur in the model atmosphere while ζ is monotonic in height.

With this method, we have reduced the problem of obtaining a hybrid σ–θ vertical coordinate to a selection of $g(\sigma)$. A suitable choice for $g(\sigma)$ is $g = 1$ virtually everywhere except a narrow region near the surface. We are currently using $g(\sigma) = (1 - e^{-\alpha\sigma})(1 - e^{-\alpha})^{-1}$, where α is a constant, with $\sigma \equiv (p_S - p)(p_S - p_T)^{-1}$. These choices yield $(\partial F/\partial p_T)_{\theta_T,p_S} = 0$ and $(\partial F/\partial p_S)_{\theta_T,p_T} = 0$ at the upper boundary. Equation (2.31) is then satisfied by $(\partial\theta_T/\partial t)_\zeta = 0$, which is a consequence of our assumption that the upper boundary is a coordinate surface.

3. Vertical discretization with the generalized vertical coordinate

a. Vertical grid

In constructing a generalized vertical coordinate model, one of the first things we have to do is choose a vertical grid. In this section we present a brief discussion on the possible choices of the vertical grid and the rationale behind our choice for the model described in this paper.

There are important advantages to the use of the Charney–Phillips grid (CP-grid; Charney and Phillips 1953) over the Lorenz grid (L-grid, Lorenz 1960) in the σ coordinate (Arakawa 1988; Arakawa and Moorthi 1988; Cullen and James 1994; Hollingsworth 1995; Arakawa and Konor 1996). These advantages of the CP-grid are directly applicable to the generalized vertical coordinate model since the model is expected to be basically a σ-coordinate model near the earth's surface.

With the θ coordinate, the thermodynamic equation reduces to a diagnostic equation for the "vertical velocity" $\dot{\theta}$. This requires that the thermodynamic equation (2.11) in the generalized vertical coordinate model be trivially satisfied when $\zeta = \theta$. In a vertically discrete system, this can be most easily done by predicting θ at the same levels that carry $\dot{\zeta}$, as is done with the CP-grid. In the grid shown in Fig. 1, which becomes the CP-grid for $P \equiv p$ (or $F \equiv \sigma$), the atmosphere is divided into L layers identified by integer indices increasing downward. These layers are bounded by $L + 1$ interfaces identified by half-integer indices. The upper and lower boundaries of the atmosphere are placed at levels with indices ½ and $L + ½$, respectively. The horizontal velocities are predicted for the layers and the potential temperature is predicted at the interfaces, where the vertical mass flux is carried.

Discretization of the hydrostatic equation in a generalized vertical coordinate is not a simple problem. In such a coordinate, determining the pressure gradient force (2.15) requires both the Montgomery potential M and the geopotential Φ at the levels where the horizontal velocity $\mathbf{v}$ is defined. Then, the simplest discretization of $\partial M/\partial\theta = \Pi$ is

$$M_l - M_{l+1} = \Pi_{l+1/2}(\theta_l - \theta_{l+1}). \tag{3.1}$$

With the CP-grid, θ_l is a specified function of $\theta_{l+1/2}$ and $\theta_{l-1/2}$. The simplest discretization of $\partial\Phi/\partial\Pi = -\theta$ is, on the other hand,

$$\Phi_l - \Phi_{l+1} = \theta_{l+1/2}(\Pi_{l+1} - \Pi_l). \tag{3.2}$$

In the θ coordinate, $\theta_{l+1/2}$ and $\theta_{l-1/2}$ (and thus θ_l and θ_{l+1}) are prescribed. Equation (3.1) then determines M for use in the pressure gradient force from predicted $\Pi_{l+1/2}$. In the σ or p coordinate, on the other hand, $\theta_{l+1/2}$ and $\theta_{l-1/2}$ are predicted. Also, it is the distribution of Φ rather than M that determines the pressure gradient force. By using $M_l = \theta_l\Pi_l + \Phi_l$, we obtain the vertically discrete form of the equation $\partial\Phi/\partial\Pi = -\theta$ that corresponds to (3.1) as

$$\Phi_l - \Phi_{l+1} = \theta_l(\Pi_{l+1/2} - \Pi_l) + \theta_{l+1}(\Pi_{l+1} - \Pi_{l+1/2}). \tag{3.3}$$

Compare (3.3) with (3.2). The vertical distribution of θ that satisfies (3.3) may include a computational mode because of the averaging necessary to obtain the right-hand side from θ at half-integer levels while (3.2) is free from such a problem. Despite this disadvantage for the σ or p coordinate, we have selected (3.1) and, correspondingly, (3.3) for the hydrostatic equations since our purpose of developing a generalized vertical coor-

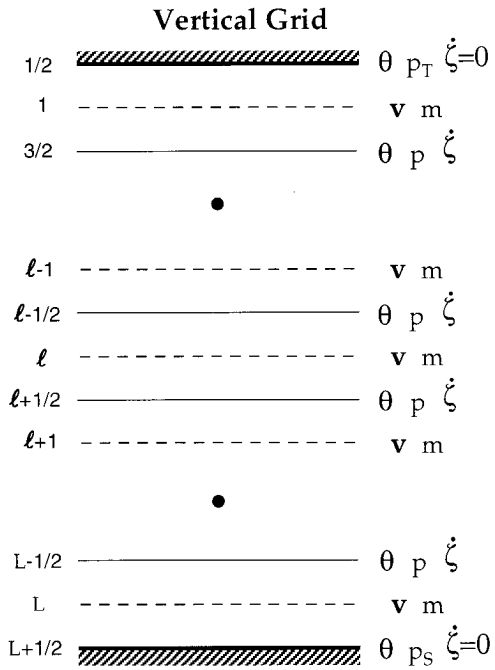

FIG. 1. Vertical grid used in the generalized vertical coordinate model.

dinate model is to take advantage of the isentropic coordinate except near the earth's surface.

b. Formulation of the vertically discrete continuity equation

We apply the continuity equation (2.5) to layer l. Then we may write

$$\frac{\partial m_l}{\partial t} + \nabla\cdot(m\mathbf{v})_l + \frac{1}{(\delta\zeta)_l}[(m\dot{\zeta})_{l+1/2} - (m\dot{\zeta})_{l-1/2}] = 0$$
$$\text{for } l = 1, 2, \ldots, L. \tag{3.4}$$

Corresponding to (2.3), we define

$$m_l \equiv -\frac{p_{l+1/2} - p_{l-1/2}}{(\delta\zeta)_l} \quad \text{for } l = 1, 2, \ldots, L, \tag{3.5}$$

where

$$(\delta\zeta)_l \equiv \zeta_{l+1/2} - \zeta_{l-1/2} \quad \text{for} \quad l = 1, 2, \ldots, L. \tag{3.6}$$

The boundary conditions (2.6) are

$$(m\dot{\zeta})_{1/2} = (m\dot{\zeta})_{L+1/2} = 0. \tag{3.7}$$

c. Formulation of the vertically discrete equations satisfying constraints 1 and 2

In this section, we present a vertically discrete system of equations that satisfies constraints 1 and 2 of Arakawa and Lamb (1977).

The model uses the pressure gradient force expressed in the form of (2.15), which can be written for layer l as

$$-(\nabla_p\Phi)_l = -\nabla M_l + \Pi_l\nabla\theta_l \quad \text{for} \quad l = 1, 2, \ldots, L. \tag{3.8}$$

Consider the mass-weighed vertical sum of (3.8), which can be rewritten using (3.5) as

$$-\sum_{l=1}^{L} m_l\nabla_p\Phi(\delta\zeta)_l$$
$$= -\nabla\sum_{l=1}^{L} m_l M_l(\delta\zeta)_l - \sum_{l=1}^{L} M_l\nabla(p_{l+1/2} - p_{l-1/2})$$
$$-\nabla\sum_{l=1}^{L} m_l\Pi_l\theta_l(\delta\zeta)_l + \sum_{l=1}^{L}\theta_l\nabla[\Pi_l(p_{l+1/2} - p_{l-1/2})]. \tag{3.9}$$

To satisfy constraint 1, the right-hand side of (3.9) must vanish when integrated along a contour of the surface topography. Since the first and third terms automatically satisfy that requirement, it remains to require that the sum of the second and fourth terms vanish. Using

$$M_l \equiv c_p T_l + \Phi_l = \Pi_l\theta_l + \Phi_l \tag{3.10}$$

and defining the Exner function for layer l by $\Pi_l \equiv f(p_{l+1/2}, p_{l-1/2})$, which yields $\nabla\Pi_l = (\partial\Pi_l/\partial p_{l+1/2})\nabla p_{l+1/2} + (\partial\Pi_l/\partial p_{l-1/2})\nabla p_{l-1/2}$, the requirement can be written as

$$-\sum_{l=1}^{L}\left[\Phi_l - \theta_l(p_{l+1/2} - p_{l-1/2})\frac{\partial\Pi_l}{\partial p_{l+1/2}}\right]\nabla p_{l+1/2}$$
$$+\sum_{l=1}^{L}\left[\Phi_l - \theta_l(p_{l+1/2} - p_{l-1/2})\frac{\partial\Pi_l}{\partial p_{l-1/2}}\right]\nabla p_{l-1/2} = 0. \tag{3.11}$$

If $p_T \equiv p_{1/2}$ = constant is used and when the dummy index l in the second term is adjusted, we can reduce (3.11) to

$$\Phi_{l+1} - \theta_{l+1}(p_{l+3/2} - p_{l+1/2})\frac{\partial\Pi_{l+1}}{\partial p_{l+1/2}}$$
$$-\Phi_l + \theta_l(p_{l+1/2} - p_{l-1/2})\frac{\partial\Pi_l}{\partial p_{l+1/2}} = 0$$
$$\text{for } l = 1, 2, \ldots, L-1 \tag{3.12}$$

and

$$\Phi_L - \theta_L(p_{L+1/2} - p_{L-1/2})\frac{\partial\Pi_L}{\partial p_{L+1/2}} = \Phi_{L+1/2}, \tag{3.13}$$

where $p_{L+1/2} \equiv p_S$ and $\Phi_{L+1/2} \equiv \Phi_S$. To obtain (3.13), we have compared the term involving $\nabla p_{L+1/2}$ in (3.11) with the term $-\Phi_S\nabla p_S$ in (2.19). Equations (3.12) and (3.13) give constraints on the discrete hydrostatic equation. The choice for $\Pi_l \equiv f(p_{l+1/2}, p_{l-1/2})$ will be made later in section 3d.

To satisfy constraint 2, we first express the work done by the pressure gradient force for each layer and identify the energy conversion term $(m\alpha\omega)$ for that layer. By multiplying (3.8) by $m_l\mathbf{v}_l$, (3.4), (3.5), and (3.10), we obtain

$$-m_l\mathbf{v}_l\cdot(\nabla_p\Phi)_l = -\nabla\cdot(\Phi_l m_l\mathbf{v}_l) + \frac{1}{(\delta\zeta)_l}$$
$$\times\left\{\Phi_{l+1/2}\left[\frac{\partial p_{l+1/2}}{\partial t} - (m\dot{\zeta})_{l+1/2}\right]\right.$$
$$\left. - \Phi_{l-1/2}\left[\frac{\partial p_{l-1/2}}{\partial t} - (m\dot{\zeta})_{l-1/2}\right]\right\} - (m\alpha\omega)_l$$
$$\text{for } l = 1, 2, \ldots, L, \tag{3.14}$$

where

$$-(m\alpha\omega)_l \equiv -\theta_l m_l\mathbf{v}_l\cdot\nabla\Pi_l + \frac{1}{(\delta\zeta)_l}$$
$$\times\left\{(\Phi_l - \Phi_{l+1/2})\left[\frac{\partial p_{l+1/2}}{\partial t} - (m\dot{\zeta})_{l+1/2}\right]\right.$$
$$\left. + (\Phi_{l-1/2} - \Phi_l)\left[\frac{\partial p_{l-1/2}}{\partial t} - (m\dot{\zeta})_{l-1/2}\right]\right\}$$
$$\text{for } l = 1, 2, \ldots, L. \tag{3.15}$$

By comparing (3.14) to (2.20), we identify (3.15) as the

discrete form of the energy conversion term. Then, if we write the discrete form of the thermodynamic energy equation (2.21) as

$$\frac{\partial(m_l c_p T_l)}{\partial t} + \nabla\cdot(c_p T_l m_l \mathbf{v}_l) + \frac{c_p}{(\delta\zeta)_l}[(Tm\dot{\zeta})_{l+1/2} - (Tm\dot{\zeta})_{l-1/2}] = (m\alpha\omega)_l + (mQ)_l \qquad \text{for } l = 1, 2, \ldots, L, \tag{3.16}$$

where $(m\alpha\omega)_l$ is given by (3.15), and if we choose

$$(c_P Tm\dot{\zeta})_{1/2} = (c_P Tm\dot{\zeta})_{L+1/2} = 0 \tag{3.17}$$

at the top and bottom boundaries, constraint 2 is satisfied regardless of the specific definitions of $(c_P Tm\dot{\zeta})_{l+1/2}$.

d. Further specifications of the vertically discrete hydrostatic equation and the thermodynamic equation

To satisfy (3.12) and (3.13), we write the discrete hydrostatic equation corresponding to $\partial\Phi/\partial\Pi = -\theta$ as

$$\left.\begin{aligned}\Phi_l - \Phi_{l+1/2} &= \theta_l(p_{l+1/2} - p_{l-1/2})\frac{\partial\Pi_l}{\partial p_{l+1/2}}\\ \Phi_{l-1/2} - \Phi_l &= \theta_l(p_{l+1/2} - p_{l-1/2})\frac{\partial\Pi_l}{\partial p_{l-1/2}}\end{aligned}\right\} \quad \text{for } l = 1, 2, \ldots, L. \tag{3.18}$$

We now substitute (3.18) into (3.15) and use the result together with (3.4) and (3.10) in (3.16) and defining $c_p T_l = \Pi_l\theta_l$. Then we obtain

$$\Pi_l\left\{m_l\frac{\partial\theta_l}{\partial t} + m_l\mathbf{v}_l\cdot\nabla\theta_l\right\} - \frac{1}{(\delta\zeta)_l}\theta_l(p_{l+1/2} - P_{l-1/2}) \times\left[\frac{\partial\Pi_l}{\partial p_{l+1/2}}(m\dot{\zeta})_{l+1/2} + \frac{\partial\Pi_l}{\partial p_{l-1/2}}(m\dot{\zeta})_{l-1/2}\right] + \frac{c_p}{(\delta\zeta)_l}[(Tm\dot{\zeta})_{l+1/2} - (Tm\dot{\zeta})_{l-1/2}] = (mQ)_l \quad \text{for } l = 1, 2, \ldots, L. \tag{3.19}$$

As discussed in section 3a, however, we wish to predict θ at half-integer levels instead of directly using (3.19). The discrete thermodynamic equation at half-integer levels can be written as

$$(m\Pi\delta\zeta)_{l+1/2}\frac{\partial\theta_{l+1/2}}{\partial t} + (\Pi m\mathbf{v}\delta\zeta)_{l+1/2}\cdot\nabla\theta_{l+1/2} + \left(\Pi\frac{\partial\theta}{\partial\zeta}\delta\zeta\right)_{l+1/2}(m\dot{\zeta})_{l+1/2} = (mQ\delta\zeta)_{l+1/2}, \quad \text{for } l = 1, 2, \ldots, L-1, \tag{3.20}$$

$$(m\Pi\delta\zeta)_{1/2}\frac{\partial\theta_{1/2}}{\partial t} + (\Pi m\mathbf{v}\delta\zeta)_{1/2}\cdot\nabla\theta_{1/2} = (mQ\delta\zeta)_{1/2}, \tag{3.21}$$

and

$$(m\Pi\delta\zeta)_{L+1/2}\frac{\partial\theta_{L+1/2}}{\partial t} + (\Pi m\mathbf{v}\delta\zeta)_{L+1/2}\cdot\nabla\theta_{L+1/2} = (mQ\delta\zeta)_{L+1/2}. \tag{3.22}$$

In (3.20)–(3.22), $(m\Pi\delta\zeta)_{l+1/2}$, $(\Pi m\mathbf{v}\delta\zeta)_{l+1/2}$, $(\Pi(\partial\theta/\partial\zeta)\delta\zeta)_{l+1/2}$ and $(mQ\delta\zeta)_{l+1/2}$ remain to be specified. Equation (3.21) is the generalized thermodynamic equation at the upper boundary. When $F = \theta$ at the upper boundary as in the choices described in section 2d to determine F, $\partial\theta_{1/2}/\partial t = 0$ replaces (3.21) to satisfy (2.31). To satisfy constraint (ii), we require that the vertical sum of $\Sigma_{l=1}^{L}$ (3.19)$(\delta\zeta)_l$ and (3.21) + $\Sigma_{l=1}^{L-1}$ (3.20) + (3.22) be identical. Then we must require

$$\sum_{l=1}^{L}\Pi_l\left(m_l\frac{\partial\theta_l}{\partial t} + m_l\mathbf{v}_l\cdot\nabla\theta_l\right)(\delta\zeta)_l = (m\Pi\delta\zeta)_{1/2}\frac{\partial\theta_{1/2}}{\partial t} + \sum_{l=1}^{L-1}(m\Pi\delta\zeta)_{l+1/2}\frac{\partial\theta_{l+1/2}}{\partial t} + (m\Pi\delta\zeta)_{L+1/2}\frac{\partial\theta_{L+1/2}}{\partial t}, \tag{3.23}$$

$$\sum_{l=1}^{L-1}\left(\Pi\frac{\partial\theta}{\partial\zeta}\delta\zeta\right)_{l+1/2} = -\sum_{l=1}^{L-1}\left[\theta_{l+1}(p_{l+3/2} - p_{l+1/2})\frac{\partial\Pi_{o+1}}{\partial p_{l+1/2}} + \theta_l(p_{l+1/2} - p_{l-1/2})\frac{\partial\Pi_l}{\partial p_{l+1/2}}\right], \tag{3.24}$$

and

$$\textstyle\sum_{l=0}^{L}(mQ\delta\zeta)_{l+1/2} = \sum_{l=1}^{L}(mQ)_l(\delta\zeta)_l. \tag{3.25}$$

Equation (3.23) can be satisfied by the following choices:

$$\theta_l \equiv \frac{1}{2}(\theta_{l+1/2} + \theta_{l-1/2}),$$

$$\text{for } l = 1, 2, \ldots, L, \tag{3.26}$$

$$(m\Pi\delta\zeta)_{l+1/2} \equiv \frac{1}{2}[\Pi_{l+1}m_{l+1}(\delta\zeta)_{l+1} + \Pi_l m_l(\delta\zeta)_l]$$

$$\text{for } l = 1, 2, \ldots, L-1, \tag{3.27}$$

$$(m\Pi\delta\zeta)_{1/2} \equiv \frac{1}{2}\Pi_1 m_1(\delta\zeta)_1, \tag{3.28}$$

$$(m\Pi\delta\zeta)_{L+1/2} \equiv \frac{1}{2}\Pi_L m_L(\delta\zeta)_L, \tag{3.29}$$

$$(\Pi m\mathbf{v}\delta\zeta)_{l+1/2} \equiv \frac{1}{2}[\Pi_{l+1}m_{l+1}\mathbf{v}_{l+1}(\delta\zeta)_{l+1} + \Pi_l m_l\mathbf{v}_l(\delta\zeta)_l]$$

$$\text{for } l = 1, 2, \ldots, L-1, \tag{3.30}$$

$$(\Pi m\mathbf{v}\delta\zeta)_{1/2} \equiv \frac{1}{2}\Pi_1 m_1\mathbf{v}_1(\delta\zeta)_1, \tag{3.31}$$

and

$$(\Pi m\mathbf{v}\delta\zeta)_{L+1/2} \equiv \frac{1}{2}\Pi_L m_L\mathbf{v}_L(\delta\zeta)_L. \tag{3.32}$$

If we choose

$$\left.\begin{aligned}\frac{\partial\Pi_l}{\partial p_{l+1/2}} &\equiv \frac{\Pi_{l+1/2}-\Pi_l}{p_{l+1/2}-p_{l-1/2}}\\ \frac{\partial\Pi_l}{\partial p_{l-1/2}} &\equiv \frac{\Pi_l-\Pi_{l-1/2}}{p_{l+1/2}-p_{l-1/2}}\end{aligned}\right\} \quad \text{for } l = 1, 2, \ldots, L, \tag{3.33}$$

we find that $\Pi_l \equiv f(p_{l+1/2}, p_{l-1/2})$ that satisfies (3.33) is

$$\Pi_l \equiv \frac{1}{1+\kappa}\frac{\Pi_{l+1/2}p_{l+1/2} - \Pi_{l-1/2}p_{l-1/2}}{p_{l+1/2} - p_{l-1/2}}$$

$$\text{for } l = 1, 2, \ldots, L, \tag{3.34}$$

which is identical to the choice for Π_l made by Phillips (1974). Equation (3.24), on the other hand, is satisfied by the choice

$$\left(\Pi\frac{\partial\theta}{\partial\zeta}\delta\zeta\right)_{l+1/2} \equiv \Pi_{l+1/2}(\theta_{l+1} - \theta_l)$$

$$\text{for } l = 1, 2, \ldots, L-1. \tag{3.35}$$

Finally, (3.25) relates the diabatic heating defined for layers and that for interfaces. In the model being described here, the moisture budget equation is applied to the layers together with the continuity equation and, consequently, the heating due to condensation of water vapor is obtained for the layers. Then it is necessary to relate the diabatic heating at the layer interfaces to that for the layers. To satisfy (3.25), which is a consequence of constraint 2, we express the diabatic heating at the layer interfaces as

$$(mQ\delta\zeta)_{l+1/2} = \frac{1}{2}[(mQ)_l(\delta\zeta)_l + (mQ)_{l+1}(\delta\zeta)_{l+1}]$$

$$\text{for } l = 1, 2, \ldots, L-1 \tag{3.36}$$

and at the upper and lower boundaries as

$$(mQ\delta\zeta)_{1/2} = \frac{1}{2}(mQ)_1(\delta\zeta)_1 \tag{3.37}$$

and

$$(mQ\delta\zeta)_{L+1/2} = \frac{1}{2}(mQ)_L(\delta\zeta)_L, \tag{3.38}$$

respectively. With the definitions given by (3.36)–(3.38), our model differs from the isentropic coordinate model developed by Arakawa and Hsu (1990) even when $\zeta \equiv \theta$.

e. Vertically discrete pressure tendency and mass flux equations

Substituting (3.5) in (3.4), summing the result multiplied by $(\delta\zeta)_l$ from $l = 1$ to l, and assuming $\partial p_T/\partial t = 0$, we can obtain the pressure tendency equation

$$\frac{\partial p_{l+1/2}}{\partial t} = \sum_{k=1}^{l}\boldsymbol{\nabla}\cdot(m_k\mathbf{v}_k)(\delta\zeta)_k + (m\dot{\zeta})_{l+1/2}$$

$$\text{for } l = 1, 2, \ldots, L, \tag{3.39}$$

where the upper boundary condition (3.7) is used. Applying (3.39) to $l = L$ and using (3.7), we obtain the surface pressure tendency equation as

$$\frac{\partial p_s}{\partial t} = \sum_{k=1}^{L}\boldsymbol{\nabla}\cdot(m_k\mathbf{v}_k)(\delta\zeta)_k. \tag{3.40}$$

f. Determination of the vertical mass flux

As discussed in section 2, one of the key issues in the formulation of the generalized vertical coordinate is the determination of vertical mass flux. In the continuous system, the vertical mass flux is determined by (2.23). In the discrete system, we similarly require that

$$\frac{\partial}{\partial t}F(\theta_{l+1/2}, p_{l+1/2}, p_s) = 0 \quad \text{for } l = 0, 1, 2, \ldots, L. \tag{3.41}$$

The procedure to satisfy (3.41) has two steps. In the first step, θ is predicted by the thermodynamic equations (3.20)–(3.22) with only the horizontal advection and diabatic heating terms retained. If we denote the predicted potential temperature by $\hat{\theta}$, this process can be written as

$$\hat{\theta}_{l+1/2} = \theta_{l+1/2} + \frac{\delta t\{(mQ\delta\zeta)_{l+1/2} - (\Pi m\mathbf{v}\delta\zeta)_{l+1/2}\cdot\boldsymbol{\nabla}\theta_{l+1/2}\}}{(m\Pi\delta\zeta)_{l+1/2}}$$

$$\text{for } l = 1, 2, \ldots, L-1, \tag{3.42}$$

where δt is the time step. In addition, the pressure p is predicted by the pressure tendency equation (3.39) with only the convergence of the horizontal mass flux retained. The surface pressure p_S is also predicted with the surface pressure tendency equation (3.40). These predictions of $\hat{p}$ and $\hat{p}_S$ follow the prediction of m through the use of a predictor–corrector sequence in the continuity equation (see appendix B). The deviation of ζ from its original value is then determined by

$$(\Delta\zeta)_{l+1/2} \equiv \hat{F}_{l+1/2} - F_{l+1/2} \quad \text{for} \quad l=1, 2, \ldots, L-1, \tag{3.43}$$

where $\hat{F}_{l+1/2} \equiv F(\hat{\theta}_{l+1/2}, \hat{p}_{l+1/2}, \hat{p}_S)$. In the second step, we require that the effects of $m\dot{\zeta}$ compensate $\Delta\zeta$ so that

$$\left[-\left(\frac{\partial\hat{F}}{\partial\hat{\theta}}\right)_{l+1/2}\left(\Pi\frac{\partial\theta}{\partial\zeta}\delta\zeta\right)_{l+1/2}(m\Pi\delta\zeta)^{-1}_{l+1/2} + \left(\frac{\partial\hat{F}}{\partial\hat{p}}\right)_{l+1/2}\right](m\dot{\zeta})_{l+1/2} = \frac{-(\Delta\zeta)_{l+1/2}}{(\delta t)} \quad \text{for } l=1, 2, \ldots, L-1. \tag{3.44}$$

Equation (3.44) gives the vertical mass flux $(m\dot{\zeta})$. It is assumed that $[\Pi(\partial\theta/\partial\zeta)\delta\zeta]_{l+1/2}(m\Pi\delta\zeta)^{-1}_{l+1/2}$ remains unchanged during these steps. To reduce the resulting errors, the above steps are iterated two or more times. In each iteration, $\hat{\theta}$ and $\hat{p}$ are replaced by $\hat{\theta} - \delta t(m\dot{\zeta})_{l+1/2}[\Pi(\partial\theta/\partial\zeta)\delta\zeta]_{l+1/2}(m\Pi\delta\zeta)^{-1}_{l+1/2}$ and $\hat{p} + \delta t(m\dot{\zeta})_{l+1/2}$, respectively.

When $\zeta = \theta$, the use of (3.42) and (3.44) in (3.20) and the assumption of $(mQ)_{L+1/2} = 0$ trivially satisfy the thermodynamic equation. For this case, the discrete pressure gradient force (3.8) also reduces to the gradient of the Montgomery potential, as in the isentropic coordinate model developed by Hsu and Arakawa (1990). Using (3.33) in (3.18), on the other hand, the discrete hydrostatic equation used in Hsu and Arakawa (1990) can also be obtained. Additionally, the definitions (3.10), (3.26), and (3.34) are identical to the ones used in their model. Therefore, the generalized vertical coordinate model described here becomes identical to Hsu and Arakawa's model for $\zeta \equiv \theta$ as long as there is no diabatic heating. Thus, the advantages of the isentropic vertical coordinate demonstrated by their model is maintained in our model. Equations (3.36)–(3.38), however, are different from (5.48) of their paper.

A summary of the system of discrete equations based on the generalized ζ coordinate is given in appendix A.

4. Horizontal and time discretization

The horizontal discretization follows Hsu and Arakawa (1990), which presents schemes especially designed to handle computational difficulties associated with an isentropic vertical coordinate. The continuity equation uses a predictor–corrector sequence in the time integration split to the zonal and meridional directions to guarantee positive definiteness and stability. The energy conserving and potential enstrophy dissipating scheme of Arakawa and Hsu (1990) is used in the momentum equation. The horizontal advection scheme for the thermodynamic equation is a generalization of the scheme for the continuity equation, which is also split in zonal and meridional directions. A summary of the horizontal schemes used in the generalized vertical coordinate model is presented in appendix B.

In the time integration of mass and potential temperature, a two-step procedure is followed to accommodate the determination of the vertical mass flux discussed in section 3f. The continuity equation consisting of only the horizontal convergence term and the thermodynamic equation consisting of only the horizontal advection and diabatic heating terms are forwarded for one time step. A simple Euler-forward scheme is used here for the thermodynamic equation. After the vertical mass flux is determined, following the procedure described in section 3f, the prediction of the mass is completed by adding the contributions due to the convergence of the vertical mass flux. The prediction of the potential temperature is also completed by adding the contribution of the vertical advection term, again using a simple Euler-forward scheme.

An ''economical explicit time difference scheme'' described by Mesinger and Arakawa (1976) is used in the pressure gradient force term of the momentum equation. In the advection of momentum, the Euler-forward scheme is used. A flowchart describing the time integration is presented in appendix C.

5. Additional features of the model

a. Dry convective adjustment

As described in section 2e, a particular formulation is used to define a hybrid $\zeta \equiv F(\theta, \sigma)$ vertical coordinate that prevents overturning of ζ surfaces even when stratification is unstable. There are, however, physical reasons not to allow unstable stratifications in the quasi-static system. In the generalized vertical coordinate model, therefore, we include a dry convective adjustment to instantly restore a neutral stratification between adjacent unstable layers. The adjustment acts when $\theta_{l-1/2} < \theta_{l+1/2}$ occurs and restores the potential temperature to $\hat{\theta}_{l-1/2} = \hat{\theta}_{l+1/2}$ in both levels. During the adjustment, the vertical sum of the mass and the mass-weighted potential temperature remain unchanged so that

$$\hat{\theta}_{l-1/2} = \hat{\theta}_{l+1/2} = \frac{\theta_{l+1/2}m_{l+1/2} + \theta_{l-1/2}m_{l-1/2}}{m_{l+1/2} + m_{l-1/2}}, \quad \text{if } \theta_{l-1/2} < \theta_{l+1/2}. \tag{5.1}$$

The pressure is also adjusted to satisfy (3.41). At present, the adjustment does not affect the velocity and mixing ratio of atmospheric constituents.

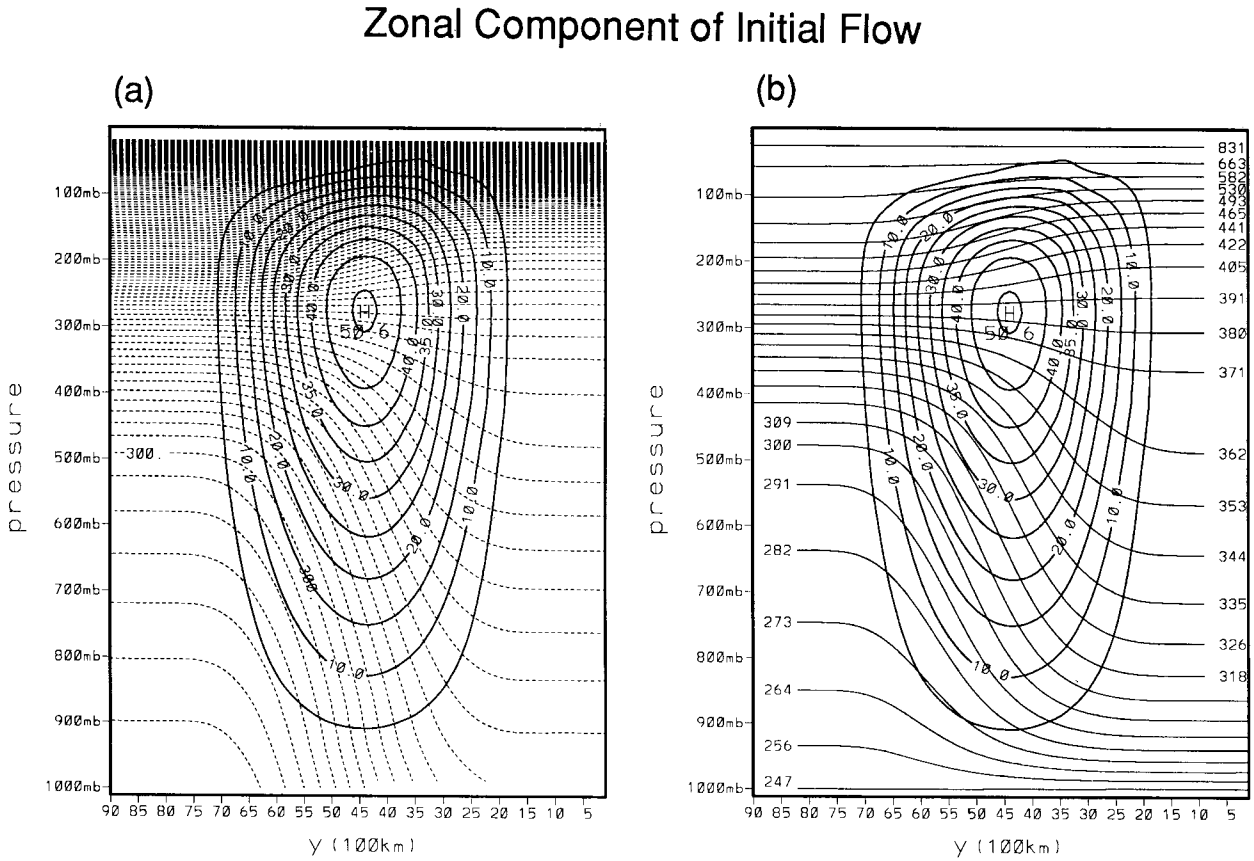

FIG. 2. Zonal component of the initial flow: zonal velocity (solid lines), (a) potential temperature (dashed lines), (b) ζ contours (thin solid lines). Contour intervals are 5 m s^{-1} for zonal velocity and 5 K for potential temperature.

b. *Vertical momentum diffusion*

To avoid generating artificially strong winds in layers with negligible mass, a vertical momentum diffusion scheme is included in the model. The diffusion acts only when the thickness of the layers becomes small. In the continuous case, the change in the momentum due to the diffusion is $\partial \mathbf{v}/\partial t = (1/\rho)\partial \boldsymbol{\tau}/\partial z$, where $\boldsymbol{\tau}$ is the horizontal stress given by $\boldsymbol{\tau} = \rho K\, \partial \mathbf{v}/\partial z$ with the diffusion coefficient K. In the discrete case, we can write

$$\hat{\mathbf{v}}_l = \mathbf{v}_l + \frac{\delta t}{\rho_l (\delta z)_l}(\hat{\boldsymbol{\tau}}_{l-1/2} - \hat{\boldsymbol{\tau}}_{l+1/2})$$

$$\text{for } l = 1, 2, \ldots, L, \tag{5.2}$$

where $\hat{\mathbf{v}}_l$ and $\hat{\boldsymbol{\tau}}_{l+1/2}$ denote $\mathbf{v}_l$ and $\boldsymbol{\tau}_{l+1/2}$ modified by the diffusion process and $(\delta z)_l \equiv z_{l-1/2} - z_{l+1/2}$. We choose

$$\hat{\boldsymbol{\tau}}_{l+1/2} \equiv \rho_{l+1/2} K^* [(\delta z)_l (\delta z)_{l+1}]^{1/2} (\hat{\mathbf{v}}_l - \hat{\mathbf{v}}_{l+1}),$$

$$\text{for } l = 1, 2, \ldots, L - 1, \tag{5.3}$$

where K^* is a constant coefficient and

$$\hat{\boldsymbol{\tau}}_{1/2} = \hat{\boldsymbol{\tau}}_{L+1/2} = 0. \tag{5.4}$$

From (5.2) and (5.3), we see that, as $(\delta z)_l \to 0$ while $(\delta z)_{l+1}$ and $(\delta z)_{l-1}$ are finite, $\hat{\mathbf{v}}_l$ approaches to an average of $\hat{\mathbf{v}}_{l+1}$ and $\hat{\mathbf{v}}_{l-1}$. Currently, we are using $K^* = 5 \times 10^{-5}$ s^{-1}.

c. *Mass restoration*

For computational reasons, the mass in each layer is not allowed to become very small. The positive-definite scheme used in the continuity equation has a built-in protection to prevent the layer mass from dropping below a prescribed lower limit during the process of horizontal mass-flux convergence (see appendix B). Diabatic heating, time-truncation, and roundoff errors can also cause the layer mass drop below the lower limit. When this occurs, an instant restoration of mass to the lower limit is performed through mass fluxes from the adjacent layers. The lower limit of mass is currently set to 1 mb.

d. *Horizontal mass and potential temperature diffusions*

In some of the simulations we performed with the model, wavelike perturbations with wavelengths of a few grid intervals developed in the lower cyclonic flank of the zonal jet. The frequency of the perturbations is

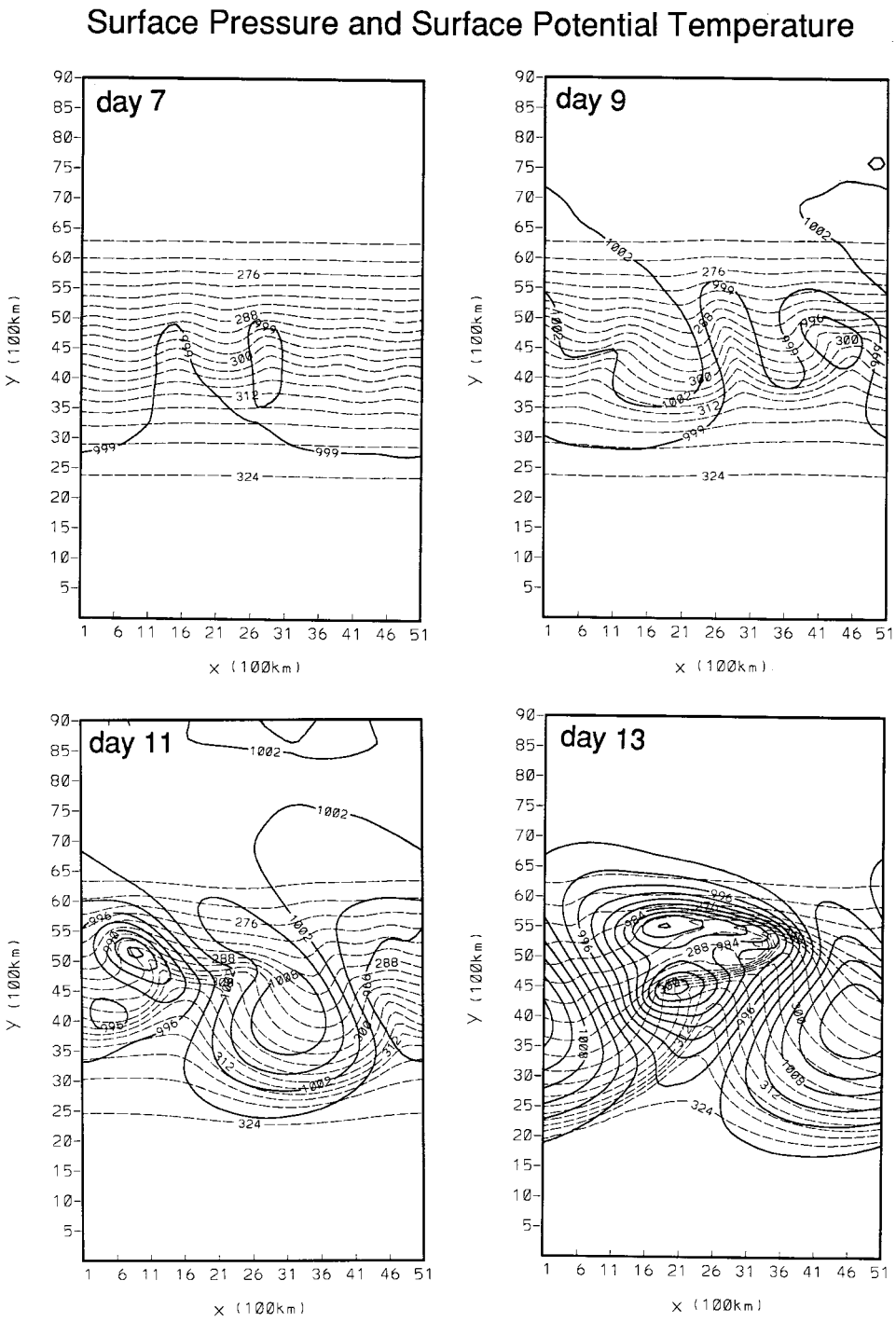

FIG. 3. Surface pressure (solid lines) and surface potential temperature (dashed lines) for day 7 to day 19. Contour intervals are 3 mb for surface pressure and 3 K for surface potential temperature.

close to that of inertial oscillations with a slow propagation in the meridional direction. We surmise that the nonnegligible amplitude of these oscillations is caused by trapping of slowly propagating inertia–gravity waves due to sharp horizontal and vertical variations of the thickness of the model layers. A horizontal mass diffusion with the diffusion coefficient 10^5 m^2 s^{-1} is added to the model to damp these oscillations.

In the thin model layers near the surface, the model has difficulties in simulating shallow inertia–gravity waves due to the use of the C-grid (see Arakawa 1988; Arakawa and Lamb 1977). To minimize these difficul-

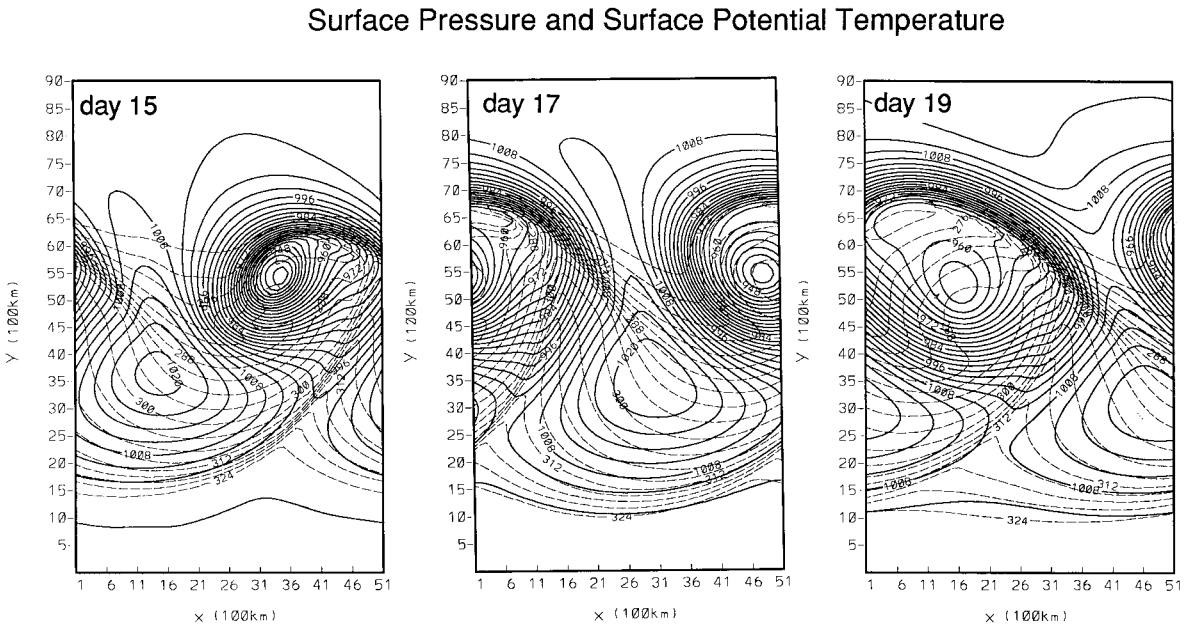

FIG. 3. (*Continued*)

ties, we also include a horizontal potential temperature diffusion with the coefficient 10^4 m^2 s^{-1}.

e. Newtonian-type heating and friction

At this stage the model does not include comprehensive physical processes. Physical processes are represented in the current version of the model by simple thermal forcing and friction. Thermal forcing is given in the form of Newtonian heating, which relaxes the thermal field to an equilibrium. In the pressure coordinate, the Newtonian heating has the form

$$Q = -\gamma c_p (T - T^*)_p, \tag{5.5}$$

where γ is a constant coefficient and T^* is the equilibrium temperature. Following (2.13) and simplifying, (5.5) can be rewritten as

$$Q = -\gamma c_p \left[(T - T^*)_\zeta - \left(\overline{\frac{\partial T}{\partial p}} \right) (p - p^*)_\zeta \right], \tag{5.6}$$

where p^* is the pressure of the equilibrium state and $(\overline{\partial T/\partial p})$ varies solely with height. The heating given by (5.6) is applied to the interfaces of the layers identified by $l + \frac{1}{2}$ for $l = 1, 2, \ldots, L$.

Friction is in the form of Rayleigh damping of momentum for the layers in the lowest 100-mb depth. Since the pressure thickness of the model layers can have large spatial and temporal variations, the friction force is determined for each model layer and each time step by

$$F_l = \kappa_V^* \min\left(1, \frac{p_{l+1/2} - p_B}{p_{l+1/2} - p_{l-1/2}}\right) \times \frac{\max(0, p_{l+1/2} - P_B)}{p_{l+1/2} - p_B} \times \mathbf{v}_l. \tag{5.7}$$

We are currently using $p_B = 0.9 p_S$ and $\kappa_V^* = 1$ day^{-1}.

6. Numerical simulation using the generalized vertical coordinate model

The performance of the generalized vertical coordinate model is tested by simulating the nonlinear evolution of midlatitude disturbances on a β plane. We have performed several simulations using different vertical and horizontal resolutions and physical parameters. Among these simulations, we have selected one for this paper. In this simulation, weak Newtonian heating is given to restore the thermal field to the zonally symmetric initial basic state. The coefficient γ in (5.6) is chosen as 0.1 day^{-1} everywhere except the surface, where the coefficient is chosen as 1 day^{-1} to mimic the effect of the surface heat flux. Also, $(\overline{\partial T/\partial p})$ in (5.6) is determined from N^2 ($\equiv g\ \partial\ \ln\theta/\partial z$) $= 10^{-4}$ s^{-2} below 400 mb and $N^2 = 2 \times 10^{-4}$ s^{-2} above it. The horizontal domain is a zonal channel bounded by two rigid walls in latitude with cyclic conditions in longitude. The horizontal domain size is 5000 km in longitude and 9000 km in latitude. The horizontal grid distance is 100 km in both directions. There are 26 layers in the vertical below $p_T = 0.01$ mb. The time interval is 1 min for this simulation. The initial conditions consist of a zonally

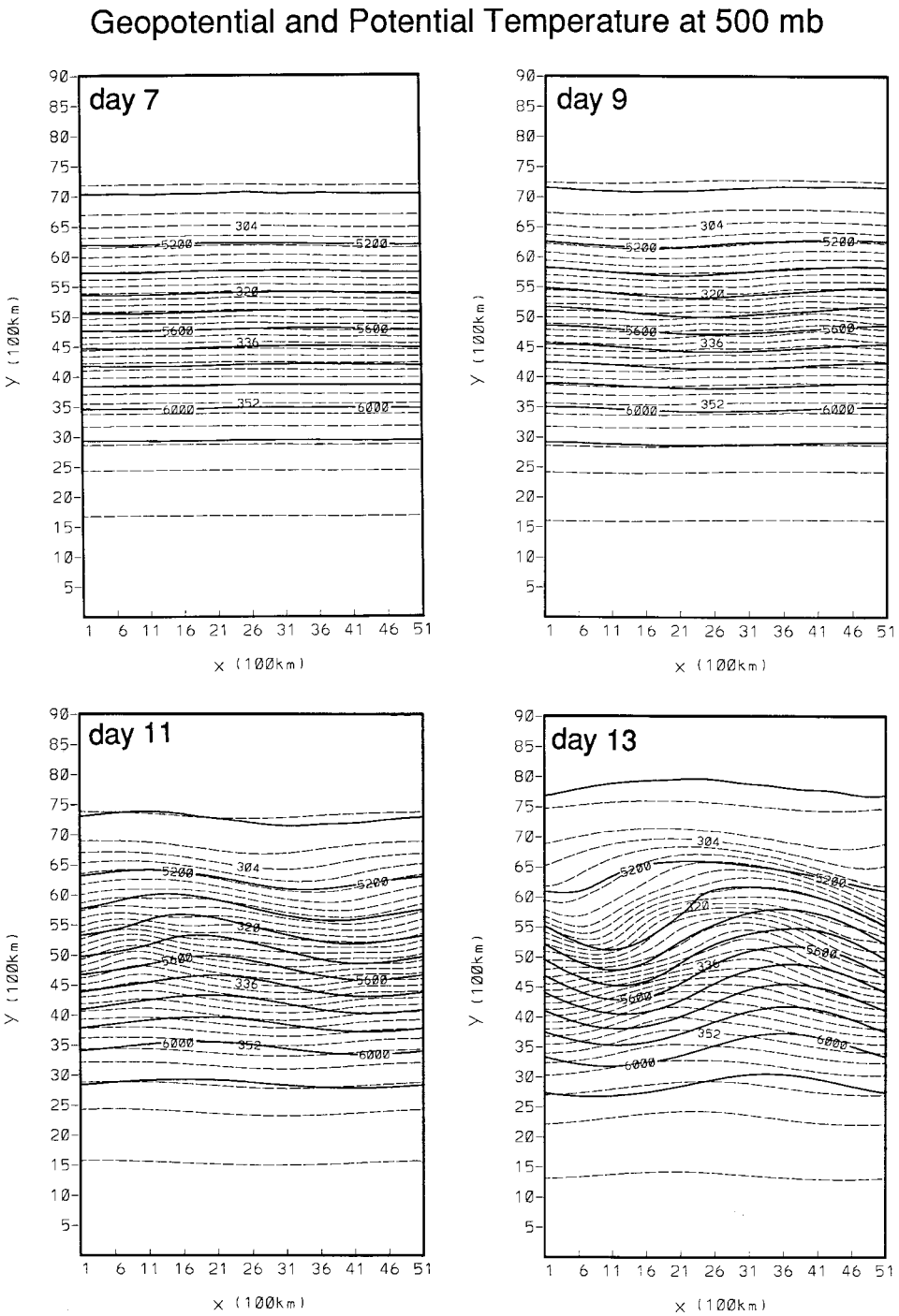

FIG. 4. Geopotential height (solid lines) and potential temperature (dashed lines) interpolated to 500 mb for day 7 to day 19. Contour intervals are 100 gpm for geopotential and 1 K for potential temperature.

uniform geostrophically balanced basic state shown in Fig. 2a and a small-amplitude *random perturbation* of potential temperature and pressure superimposed on the basic state. The hybrid vertical coordinate $\zeta \equiv F(\sigma, \theta)$ is determined following the method described in section 2e. In the determination of F, we used $\alpha = 10$, $(\partial\theta/\partial\sigma)_{\min} = -3$ K, and $\theta_{\min} = 250$ K. The vertical distribution of the coordinate surfaces for the zonal component of the initial flow is shown in Fig. 2b.

The integration is performed until day 20. The evolution of the surface pressure and surface potential temperature from days 7 to 19 is shown in Fig. 3. These

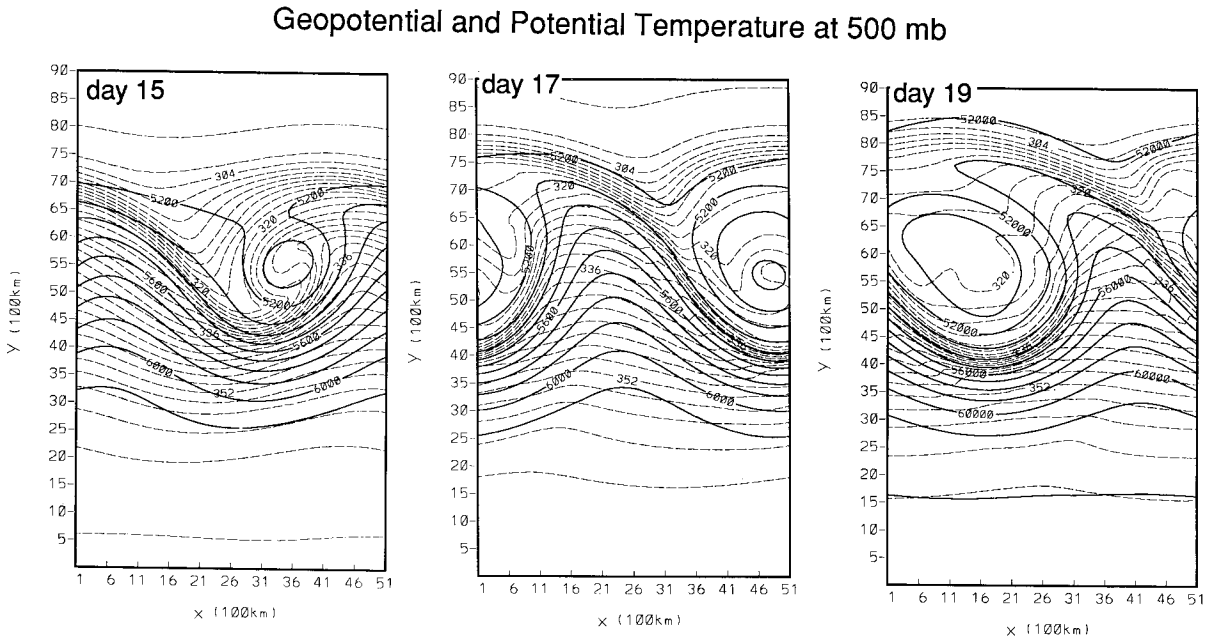

FIG. 4. (*Continued*)

fields are directly predicted in the model since the earth's surface is a coordinate surface. The geopotential height and the potential temperature on the 500-mb pressure surface for the same period are presented in Fig. 4. Interpolations from the model surfaces to the pressure surfaces are done linearly in Π. Maps of the potential vorticity (PV) on the 300-K, 320-K, and 400-K isentropic surfaces are also presented for days 7, 13, 15, and 17 in Fig. 5. To obtain the PV maps on the isentropic surfaces, the potential temperature and velocity are first interpolated linearly in Π to the isentropic surfaces and then PV is calculated from $\text{PV} \equiv -(\partial\theta/\partial p)(\mathbf{k}\cdot\nabla_\theta \times \mathbf{v} + f)$.

Figure 3 shows the growth of basically two waves; one is a short wave with approximately 1000-km wavelength, the other is a domain-size long wave. The former is a shallow wave with its largest amplitudes at the surface, and it grows faster and matures earlier than the long wave. As a result of these two growing modes, we see multiple cyclone centers at the surface in the earlier stages of the disturbance growth. After day 15, however, these centers merge to form a single large cyclone. About this time, deepening in the surface cyclone stops. At 500 mb, the thermal wave lags the geopotential wave during the growing stages of the disturbance and, correspondingly, the geopotential trough tilts westward with height.

During the evolution of the flow, sharp fronts develop at the surface and at the upper levels (see Figs. 3 and 4). As the cyclone deepens at the surface, the potential temperature gradient increases in cold, warm, and bent-back warm fronts. After the cyclone starts to fill around day 15, the surface fronts gradually deteriorate. At 500 mb, an increased isobaric potential temperature gradient upstream of the geopotential trough identifies an upper-level front. Fronts also appear at the bottom and downstream of the geopotential trough after day 15.

A semi-Lagrangian view of the evolution of the flow can be obtained through the PV maps on isentropic surfaces presented in Fig. 5. In these figures, the intersections of the 300-K and 320-K isentropic surfaces with the earth's surface are marked by plotting the 300-K and 320-K surface potential temperature contours. At the mature stage of the disturbance, PV maps on the 300-K isentropic surface show two separate intrusions of high PV air into the lower troposphere, one of which originates at the earth's surface and the other at the polar middle troposphere. The appearance of PV maxima at the earth's surface is difficult to explain. To search for its cause, we have performed additional simulations. In the simulations without diabatic heating and friction, PV maxima also appear. When the vertical resolution is increased, however, the magnitudes of the maxima become small. This evidence suggests that the origin of the PV maxima at the earth's surface is at least partially computational. One possible cause is the following. Coordinate surfaces near the earth's surface greatly deviate from isentropic surfaces. Prediction of the PV, therefore, is subject to large, noncompensating, horizontal and vertical truncation errors, resulting in poor conservation of the PV on isentropic surfaces.

The PV maps on the 320-K and 400-K isentropic surfaces also show the intrusion of a tongue of high-PV air originating from the stratosphere into the troposphere. The tongue of high PV is later cut off forming a separate cyclonic vortex. This scenario is similar to that described by Hoskins et al. (1985). As the tongue of high-PV air extends farther on the 400-K isentropic

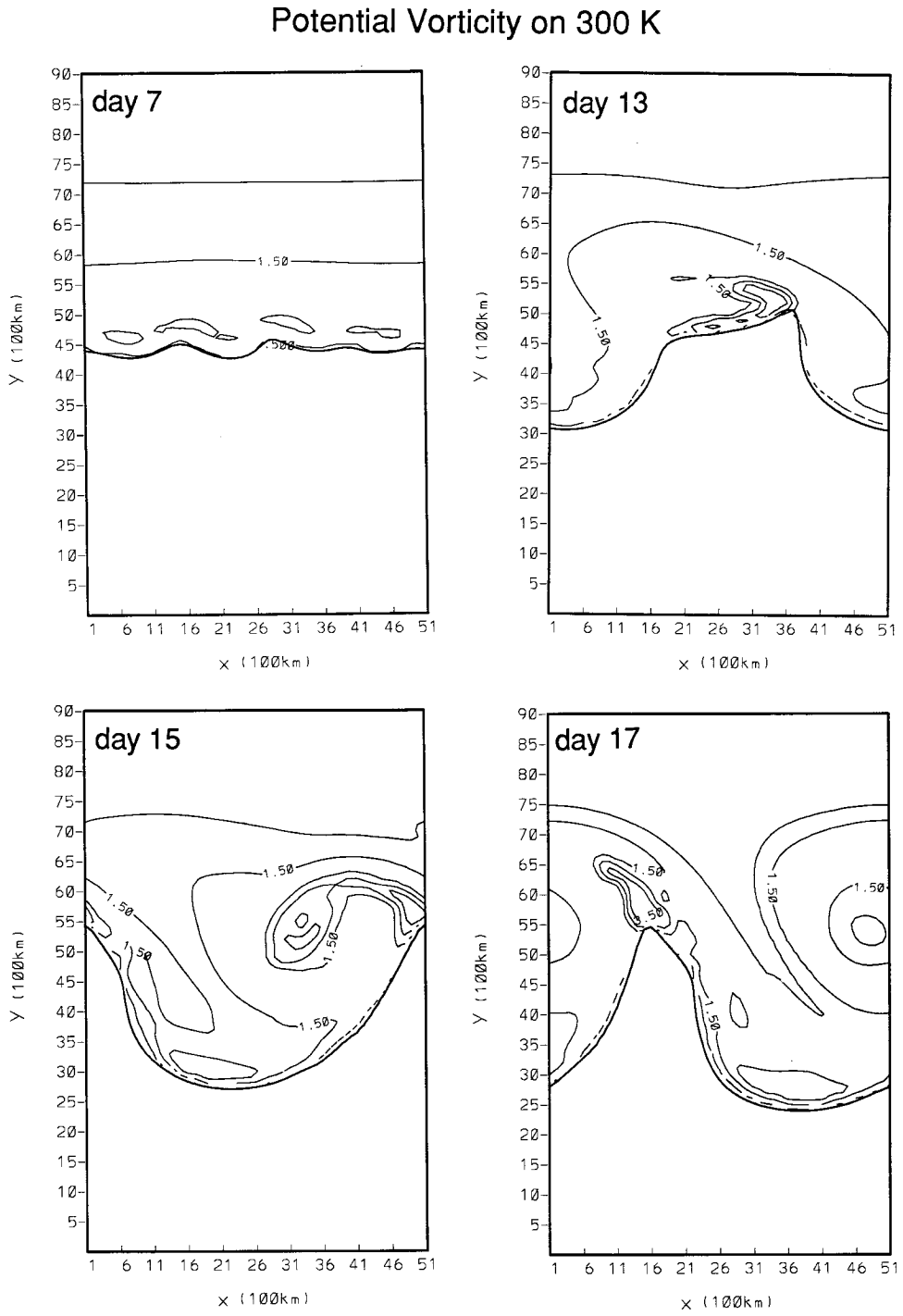

FIG. 5. Potential vorticity (PVU) on 300-K, 320-K, and 400-K isentropic surfaces for days 7, 13, 15, and 17. Contour interval is 1 PVU and the lowest contour value is 0.5 PVU. On 300-K and 320-K isentropic surfaces, the intersections with the earth's surface are marked by 300-K and 320-K surface potential temperature contours, respectively.

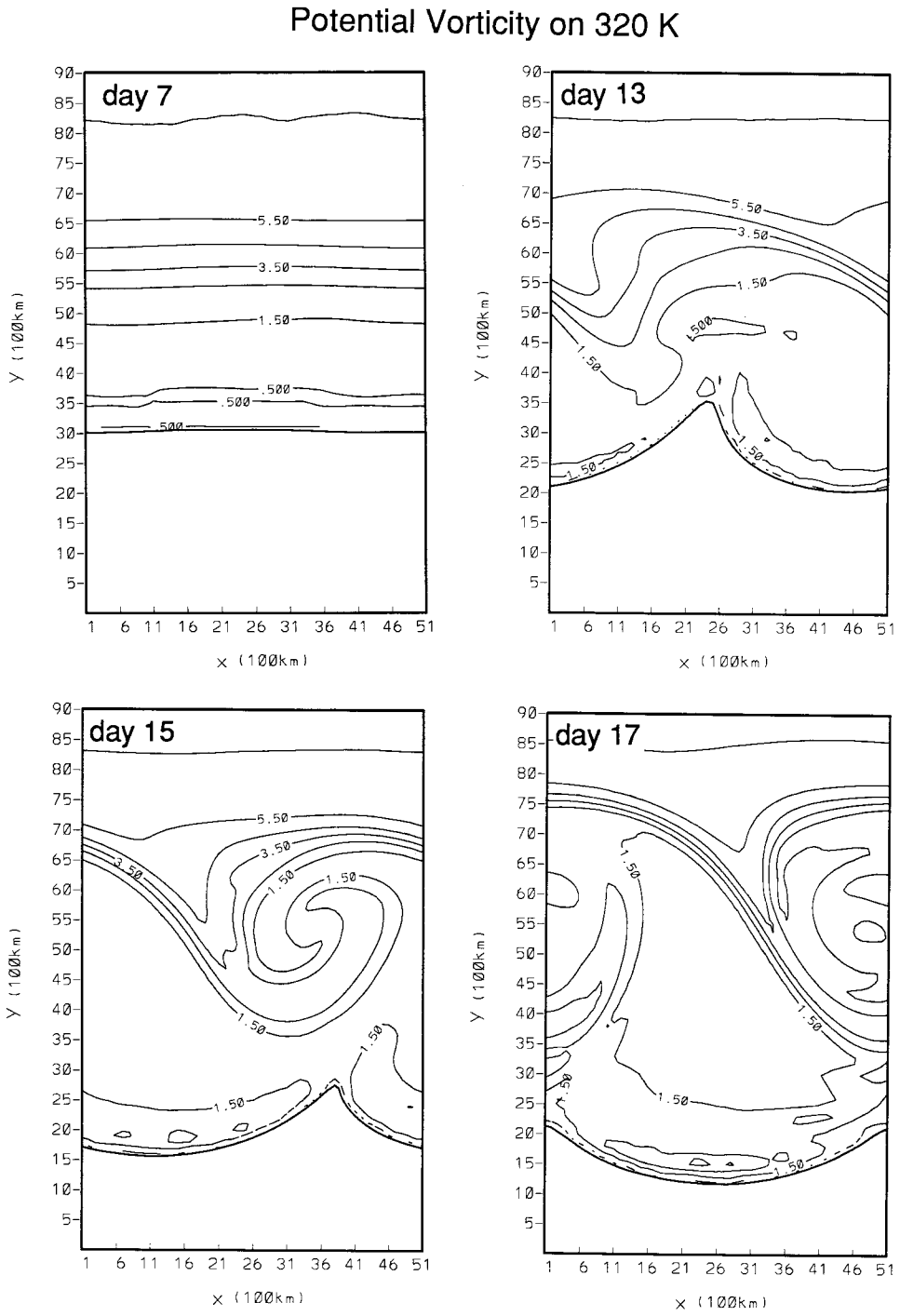

FIG. 5. (*Continued*)

surface, PV gradients intensify on the warm flank of the tongue, forming a frontlike feature. The geometric similarities between this feature and the upper-level front seen on the 500-mb chart suggest that the same dynamical process is responsible for both.

To obtain a three-dimensional view of the flow, we present in Fig. 6 selected north–south cross sections of the PV and ζ surfaces for days 7, 13, 15, and 17. The north–south cross sections are selected at $I = 6$ for day 7, $I = 46$ for day 13, $I = 31$ for day 15, and $I = 46$ for day 17, where I is the longitudinal gridpoint index. It should be noted that ζ is virtually θ everywhere except in a shallow region near the surface and, therefore, ζ presented in Fig. 6 basically describes the potential tem-

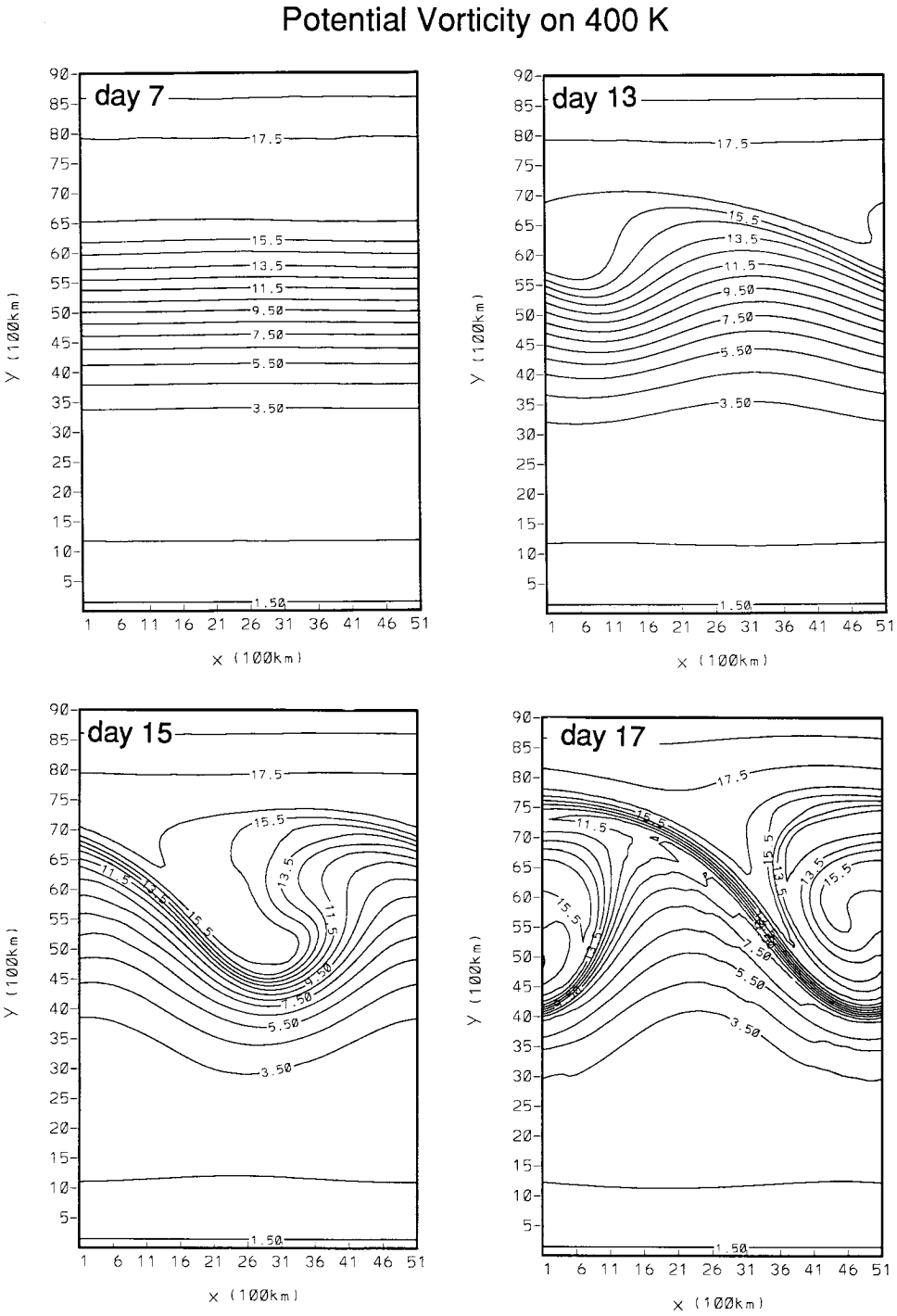

FIG. 5. (*Continued*)

perature field. On day 7, the fields appear undisturbed. The situation is different on day 13, however, when steep isentropic surfaces appear near the center of the channel at 500 mb, indicating the formation of an upper-level front. Extending along the upper-level front, a tongue of high potential vorticity from the lower stratosphere to the troposphere can be seen. On the warm flank of the tongue and above, the horizontal gradient of PV is strong. While the development continues on day 15 at upper levels, a PV maximum becomes visible at the surface. On day 17, the tongue of high PV becomes narrower and extends deeper into the troposphere along the mature upper-level front. The sharp PV gradient seen in the stratosphere in this figure corresponds

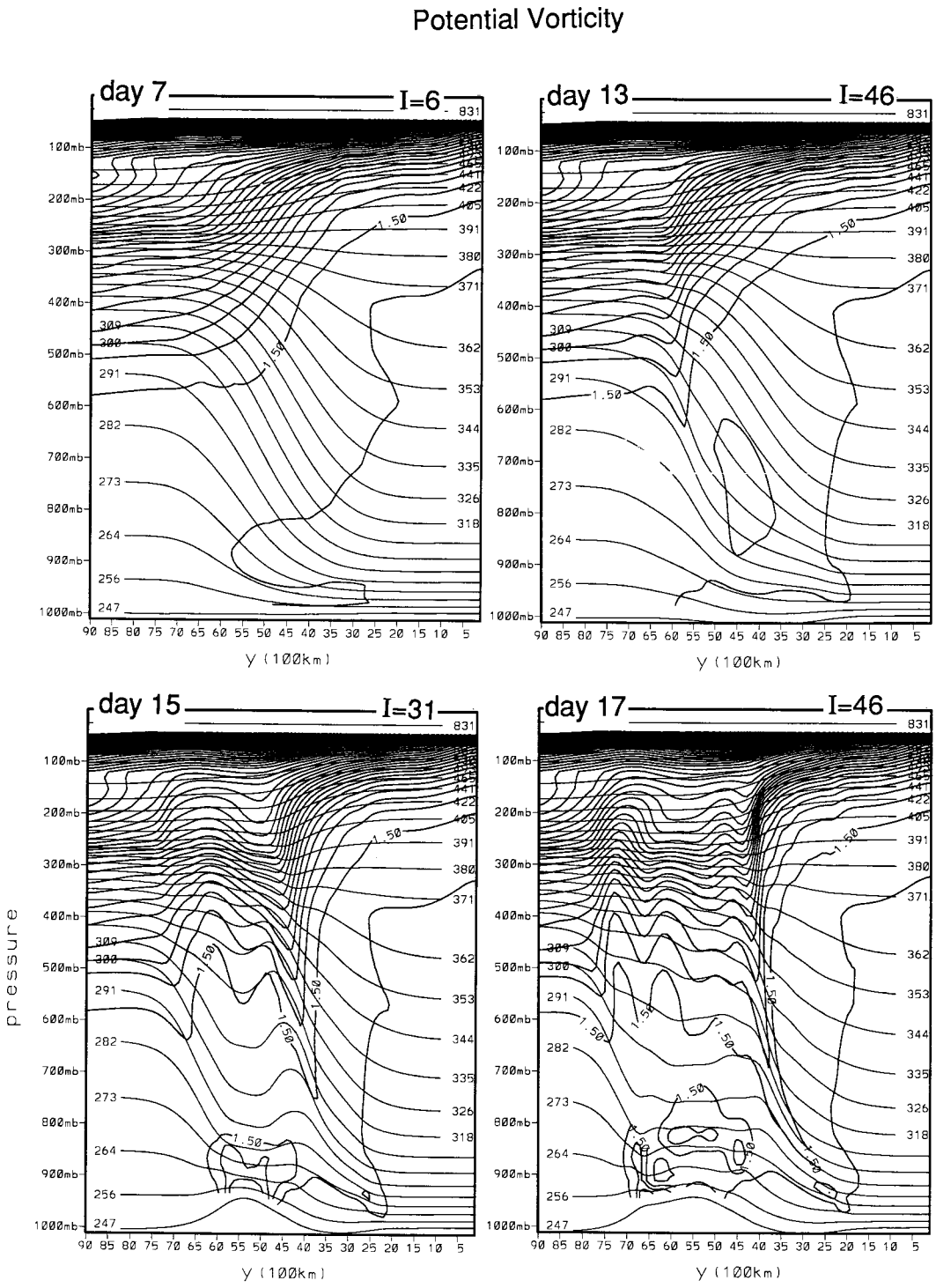

FIG. 6. North–south cross sections of the potential vorticity (PVU, thick solid lines) and ζ surfaces (thin solid lines) for days 7, 13, 15, and 17. The north–south cross sections are selected at $I = 6$ for day 7, $I = 46$ for day 13, $I = 31$ for day 15, and $I = 46$ for day 17, where I is the longitudinal gridpoint index. Contour interval is 1 PVU and the lowest contour value is 0.5 PVU.

to the frontlike feature that appears on the 400-K isentropic surface. Here a link between this feature and the upper-level front is apparent.

7. Summary and conclusions

In this paper, we have presented a numerical model of the atmosphere based on the generalized vertical coordinate $\zeta \equiv F(\theta, p, p_S)$, where ζ is a monotonic function of height, which can be the pressure p; the normalized pressure, such as p/p_S; the potential temperature θ; or any hybrid combination of all. The primary purpose for using the generalized coordinate is to combine the advantages of the isentropic coordinate away from the earth's surface with those of the σ coordinate near the surface with a smooth transition between the θ and σ domains. A simple procedure to choose $\zeta \equiv F(\theta, p, p_S)$, which guarantees that ζ is a monotonic function of height even when unstable stratifications occur, is described.

In the generalized coordinate model described in this paper, both p and θ are predicted on each coordinate surface. One of the key features of the model is the requirement of $(\partial/\partial t)_\zeta F(\theta, p, p_S) = 0$, which is used to determine the vertical mass flux. Without satisfying this requirement, $\zeta \equiv F(\theta, p, p_S)$ of a coordinate surface may change in time, and, consequently, crossing of coordinate surfaces may occur even when ζ is initially a monotonic function of height.

The Charney–Phillips grid is used as the vertical grid of the model. One of the most important advantages of the grid for a model based on the generalized vertical coordinate is that the thermodynamic equation can be trivially satisfied under adiabatic conditions when $\zeta \equiv \theta$.

Discretization of the hydrostatic equation must be carefully done in a model based on the generalized vertical coordinate. In such a coordinate, determining the pressure gradient force requires both the Montgomery potential and the geopotential at the layers where the horizontal velocity is defined. However, the most advantageous discretization for determining the Montgomery potential leads to a disadvantageous discretization for determining the geopotential, or vice versa. Since our purpose in using the generalized vertical coordinate is primarily to take advantage of the isentropic coordinate, we choose the former.

The vertical discretization of the model maintains two important integral constraints on the continuous system. These constraints are 1) the vertically integrated pressure gradient force generates no circulation along a contour of topography, and 2) the globally integrated total energy is conserved under adiabatic frictionless conditions.

The horizontal differencing schemes used in the continuity and momentum equations are especially designed for the isentropic coordinate model developed by Arakawa and Hsu (1990) and Hsu and Arakawa (1990). In the continuity equation, a positive-definite scheme is used to handle the layers with small mass. The horizontal scheme used in the momentum equation can dissipate potential enstrophy while it conserves kinetic energy. The scheme for predicting the potential temperature is newly designed to maintain the consistency between the horizontal advection of potential temperature and that of mass.

In the time discretization, a scheme is used to accommodate the procedure to determine the vertical mass flux. The scheme first predicts the mass and potential temperature due to the convergence of horizontal mass flux in the continuity equation, and the horizontal advection of the potential temperature in the thermodynamic equation. Then the vertical mass flux is determined to preserve the value of ζ at each coordinate surface. The prediction of these variables is completed by adding the contributions of the convergence of vertical mass flux in the continuity equation and the vertical advection of potential temperature in the thermodynamic equation.

The model described here includes dry convective adjustment to restore neutral stratification between adjacent unstable layers. Vertical momentum diffusion is included to avoid artificially strong velocities in the regions with negligible mass. The diffusion acts only when the thickness of the layers becomes very small. Horizontal mass diffusion is added to the model to suppress the oscillations caused by trapping of slowly propagating inertia–gravity waves due to sharp horizontal and vertical variations of the thickness of the model layers. To ease the difficulties in simulating shallow inertia–gravity waves due to the use of the C-grid, horizontal potential temperature diffusion is also added. Physical processes are represented in the current version of the model by a simple thermal forcing in the form of Newtonian heating and friction in the form of Rayleigh damping of momentum near the earth's surface.

The nonlinear evolution of a midlatitude disturbance and associated frontogenesis simulated by the model on a β plane is presented. The initial conditions consist of a zonally uniform geostrophically balanced basic state and a small-amplitude *random perturbation* of potential temperature and pressure superimposed on the basic state. Analysis of the simulated fields shows a realistic evolution of the baroclinic disturbance. During the evolution, sharp fronts are generated in the upper and middle troposphere and at the surface. The nonlinear evolution is also illustrated using potential vorticity maps on isentropic surfaces. During the evolution, deep and narrow tropopause folds along the fronts in the upper and middle troposphere are also illustrated.

We have performed several comparison simulations using the generalized vertical coordinate model and a sigma vertical coordinate model. The sigma model used in these simulations is described by Arakawa and Konor (1996), which is based on the Charney–Phillips-type vertical grid. Examples of such comparisons are given by Arakawa et al. (1994), Arakawa and Konor (1994), and Konor et al. (1994). One of the conclusions of these tests is that the generalized vertical coordinate model is able to capture the details of the surface and upper-level

frontogenesis using moderate horizontal and vertical resolutions better than the σ-coordinate model.

These simulations were performed also with different formulations of vertical momentum, horizontal potential temperature, and mass diffusions. With the formulations and coefficients described in this paper, these diffusion terms appear to have only small effects on the prevailing dynamical processes during the nonlinear evolution of extratropical cyclones. The model has also been tested by simulating cyclone evolution in the presence of surface orography with no major computational difficulty.

We are currently working on a spherical version of the generalized vertical coordinate model. We also plan to implement more comprehensive physical processes in the model.

Acknowledgments. We wish to thank Dr. Carlos R. Mechoso for his support and encouragement. We also thank two anonymous reviewers for their useful comments. Thanks are extended to Dr. John Farrara for carefully reading the manuscript and for suggesting changes to improve the manuscript. This research is funded under NSF ATM-9224863 and -9114850, NASA NAG5-2591, and DOE-CHAMMP-FG03-91ER61214. Computations are performed at computer facilities at NCAR and UCLA Department of Atmospheric Sciences.

APPENDIX A

A Summary of the Vertically Discrete System of Equations Based on the Generalized $\zeta = F(\theta, p, p_s)$ Vertical Coordinate

Continuity equation:

$$\frac{\partial m_l}{\partial t} + \nabla\cdot(m\mathbf{v})_l + \frac{1}{(\delta\zeta)_l}[(m\dot{\zeta})_{l+1/2} - (m\dot{\zeta})_{l-1/2}] = 0$$

$$\text{for } l = 1, 2, \ldots, L, \tag{A.1}$$

where

$$m_l = -(p_{l+1/2} - p_{l-1/2})(\delta\zeta)_l^{-1},\ (\delta\zeta)_l = \zeta_{l+1/2} - \zeta_{l-1/2}$$

for $l = 1, 2, \ldots, L$.

Boundary conditions:

$$(m\dot{\zeta})_{1/2} = (m\dot{\zeta})_{L+1/2} = 0. \tag{A.2}$$

Thermodynamic equation:

$$\frac{1}{2}[m_{l+1}\Pi_{l+1}(\delta\zeta)_{l+1} + m_l\Pi_l(\delta\zeta)_l]\frac{\partial\theta_{l+1/2}}{\partial t} + \frac{1}{2}[m_{l+1}\Pi_{l+1}\mathbf{v}_{l+1}(\delta\zeta)_{l+1} + m_l\Pi_l\mathbf{v}_l(\delta\zeta)_l]\cdot\nabla\theta_{l+1/2} + \Pi_{l+1/2}(\theta_{l+1} - \theta_l)(m\dot{\zeta})_{l+1/2} = (mQ\delta\zeta)_{l+1/2}$$

$$\text{for } l = 1, 2, \ldots, L-1. \tag{A.3}$$

At the boundaries,

$$\frac{1}{2}m_1\Pi_1(\delta\zeta)_1\frac{\partial\theta_{1/2}}{\partial t} + \frac{1}{2}m_1\Pi_1\mathbf{v}_1(\delta\zeta)_1\cdot\nabla\theta_{1/2} = (mQ\delta\zeta)_{1/2} \tag{A.4}$$

and

$$\frac{1}{2}m_L\Pi_L(\delta\zeta)_L\frac{\partial\theta_{L+1/2}}{\partial t} + \frac{1}{2}m_L\Pi_L\mathbf{v}_L(\delta\zeta)_L\cdot\nabla\theta_{L+1/2} = (mQ\delta\zeta)_{L+1/2}. \tag{A.5}$$

If $F = \theta$ at the upper boundary, (A.4) is replaced by $\partial\theta_{1/2}/\partial t = 0$.

Hydrostatic equation:

$$\Phi_l - \Phi_{l+1} = \theta_{l+1}(\Pi_{l+1} - \Pi_{l+1/2}) + \theta_l(\Pi_{l+1/2} - \Pi_l), \quad \text{for } l = 1, 2, \ldots, L-1. \tag{A.6}$$

At the lower boundary,

$$\Phi_L - \Phi_{L+1/2} = \theta_L(\Pi_{L+1/2} - \Pi_L), \tag{A.7}$$

where

$$\theta_l \equiv \tfrac{1}{2}(\theta_{l+1/2} + \theta_{l-1/2}) \quad \text{for} \quad l = 1, 2, \ldots, L. \tag{A.8}$$

Vertical mass flux:

$$\hat{\theta}_{l+1/2} \equiv \theta_{l+1/2} + \delta t\frac{[(mQ\delta\zeta)_{l+1/2} - (\Pi m\mathbf{v}\delta\zeta)_{l+1/2}\cdot\nabla\theta_{l+1/2}]}{(m\Pi\delta\zeta)_{l+1/2}}$$

$$\text{for } l = 1, 2, \ldots, L-1, \tag{A.9}$$

$$\hat{p}_{l+1/2} \equiv \mathcal{F}\left[p_{l+1/2},\ \delta t,\ \sum_{k=1}^{l}\nabla\cdot(m_k\mathbf{v}_k)(\delta\zeta)_k\right]$$

$$\text{for } l = 1, 2, \ldots, L-1, \tag{A.10}$$

and

$$\hat{p}_s \equiv \mathcal{F}\left[p_s,\ \delta t,\ \sum_{k=1}^{L}\nabla\cdot(m_k\mathbf{v}_k)(\delta\zeta)_k\right]. \tag{A.11}$$

Here (A.10) and (A.11) symbolically represent the predictor–corrector sequence used for the discrete continuity equation (see appendix B).

Initial estimate of the vertical mass flux:

$$(m\dot{\zeta})_{l+1/2} = -(\Delta\zeta)_{l+1/2}\left\{(\delta t)\left[-\left(\frac{\partial\hat{F}}{\partial\hat{\theta}}\right)_{l+1/2}A_{l+1/2} + \left(\frac{\partial\hat{F}}{\partial\hat{p}}\right)_{l+1/2}\right]\right\}$$

$$\text{for } l = 1, 2, \ldots, L-1, \tag{A.12}$$

where

$$(\Delta\zeta)_{l+1/2} \equiv F(\hat{\theta}_{l+1/2}, \hat{p}_{l+1/2}, \hat{p}_S) - F(\theta_{l+1/2}, p_{l+1/2}, p_S) \quad \text{for} \quad l = 1, 2, \ldots, L-1 \tag{A.13}$$

and

$$A_{l+1/2} \equiv \left(\Pi\frac{\partial\theta}{\partial\zeta}\delta\zeta\right)_{l+1/2}(m\Pi\delta\zeta)^{-1}_{l+1/2}$$

$$\text{for } l = 1, 2, \ldots, L-1. \tag{A.14}$$

The final value of the vertical mass flux is obtained by repeating (A.12) with (A.13) two or more times by replacing $\hat{\theta}_{l+1/2}$ by $\hat{\theta}_{l+1/2} - \delta t(m\dot{\zeta})_{l+1/2}A_{l+1/2}$ and $\hat{p}_{l+1/2}$ by $\hat{p}_{l+1/2} + \delta t(m\dot{\zeta})_{l+1/2}$.

Horizontal pressure gradient force:

$$-(\nabla_p\Phi)_l = -\nabla M_l + \Pi_l\nabla\theta_l \quad \text{for} \quad l = 1, 2, \ldots, L, \tag{A.15}$$

where $M_l \equiv \Phi_l + \Pi_l\theta_l$.

Exner function at integer levels:

$$\Pi_l \equiv \frac{1}{1+\kappa}\frac{\Pi_{l+1/2}p_{l+1/2} - \Pi_{l-1/2}p_{l-1/2}}{p_{l+1/2} - p_{l-1/2}}$$

$$\text{for } l = 1, 2, \ldots, L, \tag{A.16}$$

where $\Pi_{l+1/2} \equiv c_p(p_{l+1/2}/p_0)^\kappa$.

Diabatic heating at layer interfaces:

$$(mQ\delta\zeta)_{l+1/2} \equiv \frac{1}{2}[(mQ)_l(\delta\zeta)_l + (mQ)_{l+1}(\delta\zeta)_{l+1}]$$

$$\text{for } l = 1, 2, \ldots, L-1 \tag{A.17}$$

and at the upper and lower boundaries as

$$(mQ\delta\zeta)_{1/2} = \frac{1}{2}(mQ)_1(\delta\zeta)_1 \tag{A.18}$$

and

$$(mQ\delta\zeta)_{L+1/2} \equiv \frac{1}{2}(mQ)_L(\delta\zeta)_L. \tag{A.19}$$

APPENDIX B

Horizontal Finite-Difference Schemes Used in the Generalized Vertical Coordinate Model

a. Finite-difference schemes for the momentum and continuity equations

A detailed derivation of the finite-difference schemes can be found in Arakawa and Hsu (1990) and Hsu and Arakawa (1990), the latter of which is referred to as HA. In our description of the schemes here, we will refer to HA whenever it is necessary. These schemes are particularly derived to handle the difficulties with an isentropic coordinate model and to use the advantageous Arakawa C-grid. In Fig. B1, a portion of the C-grid for the interior points is shown.

The discrete form of the momentum equation is obtained from (7.5) to (7.17) of HA. For use in our model, $M_{i+1/2,j+1/2} - M_{i-1/2,j+1/2}$ in (7.5) of HA and $M_{i+1/2,j+1/2} - M_{i+1/2,j-1/2}$ in (7.6) of HA are replaced by

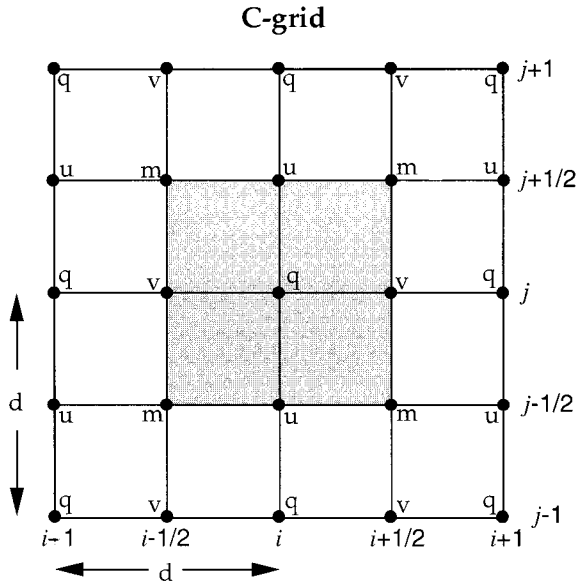

FIG. B1. A portion of the C-grid for interior grid points.

$$M_{i+1/2,j+1/2} - M_{i-1/2,j+1/2} - \frac{1}{2}(\Pi_{i+1/2,j+1/2} + \Pi_{i-1/2,j+1/2}) \times (\theta_{i+1/2,j+1/2} - \theta_{i-1/2,j+1/2}) \tag{B.1}$$

and

$$M_{i+1/2,j+1/2} - M_{i+1/2,j-1/2} - \frac{1}{2}(\Pi_{i+1/2,j+1/2} + \Pi_{i+1/2,j-1/2}) \times (\theta_{i+1/2,j+1/2} - \theta_{i+1/2,j-1/2}), \tag{B.2}$$

respectively.

The discrete momentum equation for u points at the southern boundary is

$$\frac{\partial}{\partial t}u_{i,1/2} - \frac{\partial}{\partial t}u_{i,3/2} + \frac{1}{12}(q_{i,1} + q_{i+1,1})(u^*_{i,3/2} + u^*_{i+1,3/2}) - \frac{1}{12}(q_{i-1,1} + q_{i,1})(u^*_{i-1,3/2} + u^*_{i,3/2}) + \frac{1}{12}(q_{i,1} + q_{i,2}) \times (\mathbf{v}^*_{i-1/2,2} + \mathbf{v}^*_{i+1/2,2}) - \frac{1}{24}(q_{i+1,2} + q_{i,1}) \times (\mathbf{v}^*_{i+1/2,2} + u^*_{i,3/2} + u^*_{i+1,3/2}) - \frac{1}{24}(q_{i-1,2} + q_{i,1}) \times (\mathbf{v}^*_{i-1/2,2} - u^*_{i,3/2} - u^*_{i-1,3/2}) = 0, \tag{B.3}$$

where

$$q_{i,1} \equiv \frac{f + \frac{2}{d}(u_{i,1/2} - u_{i,3/2})}{\frac{1}{2}(m_{i+1/2,3/2} + m_{i-1/2,3/2})}, \tag{B.4}$$

where d is the grid distance. At the northern boundary, (B.3) and (B.4) are symmetrically applied.

The discrete form of the continuity equation is identical to (6.1) of HA. The convergence of horizontal mass fluxes is given by (6.2) of HA, and the horizontal mass fluxes are described in (6.3) and (6.4) of HA. The time integration of the continuity equation is described in (6.5)–(6.16) of HA, in which m_i, $\mathcal{F}_{i+1/2}$, $u_{i+1/2}$, and $F_{i+1/2}$ must be replaced by $m_{i+1/2}$, $\mathcal{F}_{i+1}$, u_{i+1}, and F_{i+1}, respectively. Equation (6.15) and (6.16) are replaced by

$$\gamma^+_{i+1/2} = \hat{\gamma}^+_{i+1/2} = \left[\frac{(|m^n_{i-1} - 2m^n_i + m^n_{i+1}| + \varepsilon)^2}{(|m^n_{i-1} - 2m^n_i + m^n_{i+1}| + \varepsilon)^2 + (m^n_i - m_{\min})(m^n_{i+1} - m_{\min})}\right]^2 \tag{B.5}$$

and

$$\gamma^-_{i+1/2} = \hat{\gamma}^-_{i+1/2} = \left[\frac{(|m^n_i - 2m^n_{i+1} + m^n_{i+2}| + \varepsilon)^2}{(|m^n_i - 2m^n_{i+1} + m^n_{i+2}| + \varepsilon)^2 + (m^n_i - m_{\min})(m^n_{i+1} - m_{\min})}\right]^2, \tag{B.6}$$

respectively, introducing a small positive constant ε. Here $m_{\min}$ is the lower limit for the mass, which is currently determined for each layer from $(\delta p)_{\min} = 1$ mb. To guarantee the positive definiteness, F is limited by

$$\left.\begin{aligned} F_i &\le \frac{\delta t}{d}(m^n_{i-1} - m_{\min}) \qquad \text{for } F_i > 0 \\ -F_i &\le \frac{\delta t}{d}(m^n_i - m_{\min}) \qquad \text{for } F_i < 0 \end{aligned}\right\}, \tag{B.7}$$

where F corresponds to the horizontal mass flux u^* (or $\mathbf{v}^*$).

b. *Finite-difference schemes for the horizontal advection of the potential temperature*

The terms responsible for the horizontal advection of the potential temperature for time-continuous case are given by

$$\frac{\partial \theta_{i+1/2,j+1/2}}{\partial t} = -\left(u\frac{\partial \theta}{\partial x}\right)_{i+1/2,j+1/2} - \left(\mathbf{v}\frac{\partial \theta}{\partial y}\right)_{i+1/2,j+1/2}. \tag{B.8}$$

The advection scheme for (B.8) is derived from the scheme used in the continuity equation given by (6.5)–(6.16) of HA, so that the prediction of the mass-weighted potential temperature is consistent with that of mass. In the derivation, we used $\beta^\pm = \hat{\beta}^\pm = 1$ and $\alpha = 1/6$ in (6.10) of HA. As in the continuity equation, the scheme is split in the x and y directions, first the advection in the x direction:

$$\begin{aligned}\left(u\frac{\partial \theta}{\partial x}\right)_{i+1/2} \equiv \frac{1}{6d}\Bigg[&2\frac{m_{i+3/2}}{m_{i+1/2}}(\theta_{i+3/2} - \theta_{i+1/2})u^+_{i+1} \\ &+ \frac{m_{i-1/2}}{m_{i+1/2}}(\theta_{i+1/2} - \theta_{i-1/2})(\hat{u}^+_{i+1} + 4u^+_i + \hat{u}^+_i) \\ &- \frac{m_{i-3/2}}{m_{i+1/2}}(\theta_{i+1/2} - \theta_{i-3/2})\hat{u}^+_i \\ &+ 2\frac{m_{i-1/2}}{m_{i+1/2}}(\theta_{i+1/2} - \theta_{i-1/2})u^-_i \\ &+ \frac{m_{i+3/2}}{m_{i+1/2}}(\theta_{i+3/2} - \theta_{i+1/2})(4u^-_{i+1} + \hat{u}^-_{i+1} + \hat{u}^-_i) \\ &- \frac{m_{i+5/2}}{m_{i+1/2}}(\theta_{i+5/2} - \theta_{i+1/2})\hat{u}^-_{i+1}\Bigg],\end{aligned} \tag{B.9}$$

where the index $j + 1/2$ is omitted for simplification. An intermediate value for θ is defined as

$$\theta^*_{i+1/2,j+1/2} \equiv \theta_{i+1/2,j+1/2} - \delta t\left(u\frac{\partial \theta}{\partial x}\right)_{i+1/2,j+1/2}. \tag{B.10}$$

The advection in y direction is

$$\begin{aligned}\left(\mathbf{v}\frac{\partial \theta}{\partial y}\right)_{j+1/2} \equiv \frac{1}{6d}\Bigg[&2\frac{m_{j+3/2}}{m_{j+1/2}}(\theta^*_{j+3/2} - \theta^*_{j+1/2})\mathbf{v}^+_{j+1} + \frac{m_{j-1/2}}{m_{j+1/2}}(\theta^*_{j+1/2} - \theta^*_{j-1/2})(\hat{\mathbf{v}}^+_{j+1} + 4\mathbf{v}^+_j + \hat{\mathbf{v}}^+_j) - \frac{m_{j-3/2}}{m_{j+1/2}}(\theta^*_{j+1/2} - \theta^*_{j-3/2})\hat{\mathbf{v}}^+_j \\ &+ 2\frac{m_{j-1/2}}{m_{j+1/2}}(\theta^*_{j+1/2} - \theta^*_{j-1/2})\mathbf{v}^-_j + \frac{m_{j+3/2}}{m_{j+1/2}}(\theta^*_{j+3/2} - \theta^*_{j+1/2})(4\mathbf{v}^-_{j+1} + \hat{\mathbf{v}}^-_{j+1} + \hat{\mathbf{v}}^-_j) - \frac{m_{j+5/2}}{m_{j+1/2}}(\theta^*_{j+5/2} - \theta^*_{j+1/2})\hat{\mathbf{v}}^-_{j+1}\Bigg],\end{aligned} \tag{B.11}$$

where the index $i + \frac{1}{2}$ is omitted for simplification and

$$\left.\begin{aligned}\{\hat{u}_k^+,\ \hat{\mathbf{v}}_k^+\} &\equiv \{(u_k^+ u_{k-1}^+)^{1/2},\ (\mathbf{v}_k^+ \mathbf{v}_{k-1}^+)^{1/2}\}\\ \{\hat{u}_k^-,\ \hat{\mathbf{v}}_k^-\} &\equiv \{-(u_k^- u_{k+1}^-)^{1/2},\ -(\mathbf{v}_k^- \mathbf{v}_{k+1}^-)^{1/2}\}\end{aligned}\right\}. \quad \text{(B.12)}$$

The right-hand side of (B.8) is obtained by summing (B.9) and (B.11). At the southern boundary, for example, $\theta_{i+1/2,1/2} = \theta_{i+1/2,3/2}$, $\mathbf{v}_{i+1/2,2} = 0$ is assumed in (B.11). These boundary conditions are symmetrically applied to the equations at the northern boundary. In (B.9) and (B.11), the mass at the interfaces is defined by

$$m_{l+1/2} \equiv \frac{(\delta\zeta)_{l+1} m_{l+1} + (\delta\zeta)_l m_l}{(\delta\zeta)_{l+1} + (\delta\zeta)_l}$$

$$\text{for } l = 1, 2, \ldots, L \quad \text{(B.13)}$$

and

$$m_{1/2} \equiv m_1, \text{ and } m_{L+1/2} \equiv m_L. \quad \text{(B.14)}$$

APPENDIX C

Time Integration Scheme Used in the Generalized Vertical Coordinate Model

1) Horizontal mass fluxes (HMF) and prediction of mass due to the convergence of HMF (following appendix B):

$$\mathbf{v}^{*(n)} = \mathcal{F}\{\mathbf{v}^{(n)}, m^{(n)}\}$$

$$m_H^{(n+1)} = m^{(n)} + (\delta t)\mathcal{F}\{\mathbf{v}^{*(n)}\}.$$

2) Prediction of θ due to the horizontal advection (following appendix B):

$$\theta_H^{(n+1)} = \theta^{(n)} + (\delta t)\mathcal{F}\{\theta^{(n)}, m^{(n)}, \mathbf{v}^{(n)}\}.$$

3) Determination of the vertical mass flux (VMF) (following appendix A):

$$(m\dot{\zeta})^{(n)} = \mathcal{F}\{\theta_H^{(n+1)}, \theta^{(n)}, m_H^{(n+1)}, m^{(n)}, \mathbf{v}^{(n)}, \mathbf{v}^{*(n)}\}.$$

4) Completion of the prediction of mass by adding the contribution of convergence of VMFs (following appendix A):

$$m^{(n+1)} = m_H^{(n+1)} + (\delta t)\mathcal{F}\{(m\dot{\zeta})^{(n)}\}.$$

5) Completion of the prediction of θ by adding the contribution of vertical advection (following appendix A):

$$\theta^{(n+1)} = \theta_H^{(n+1)} + (\delta t)\mathcal{F}\{m^{(n)}, \theta^{(n)}, (m\dot{\zeta})^{(n)}\}.$$

6) Kinetic energy, potential vorticity, and pressure gradient force (following appendix A and appendix B):

$$K^{(n)} = \mathcal{F}\{\mathbf{v}^{(n)}\}$$

$$q^{(n+1)} = \mathcal{F}\{\mathbf{v}^{(n)}, m^{(n+1)}\}$$

$$-(\nabla_p \Phi)^{(n+1)} = \mathcal{F}\{\theta^{(n+1)}, m^{(n+1)}\}.$$

7) Prediction of momentum (following appendix A and appendix B):

$$\mathbf{v}^{(n+1)} = \mathbf{v}^{(n)} + (\delta t)\mathcal{F}\{-(\nabla_p \Phi)^{(n+1)}, \mathbf{v}^{*(n)}, K^{(n)}, q^{(n+1)}, \mathbf{v}^{(n)}, (m\dot{\zeta})^{(n)}\}.$$

8) Diffusions (following section 4):
Vertical momentum diffusion,

$$\hat{\mathbf{v}}^{(n+1)} = \mathbf{v}^{(n+1)} + (\delta t)\mathcal{F}\{\hat{\mathbf{v}}^{(n+1)}, m^{(n+1)}\}.$$

Horizontal mass diffusion,

$$\hat{m}^{(n+1)} = m^{(n+1)} + (\delta t)\mathcal{F}\{m^{(n+1)}\}.$$

Horizontal potential temperature diffusion,

$$\hat{\theta}^{(n+1)} = \theta^{(n+1)} + (\delta t)\mathcal{F}\{\theta^{(n+1)}\},$$

where the hat denotes the modified variables through the diffusion.

9) Dry convective adjustment (following section 4):

$$\hat{\hat{\theta}}^{(n+1)} = \hat{\theta}^{(n+1)} + \mathcal{F}\{\hat{\theta}^{(n+1)}, \hat{m}^{(n+1)}\}$$

$$\hat{\hat{m}}^{(n+1)} = \hat{m}^{(n+1)} + \mathcal{F}\{\hat{\theta}^{(n+1)}, \hat{m}^{(n+1)}\}.$$

REFERENCES

Arakawa, A., 1988: Finite-difference methods in climate modeling. *Physically-Based Modelling and Simulation of Climate and Climatic Change*, Part I, M. E. Schlesinger, Ed., Kluwer Academic Publisher, 79–168.

——, and V. Lamb, 1977: Computational design of the basic dynamical processes of the UCLA general circulation model. *Methods in Computational Physics*, Vol. 17, J. Chang, Ed., Academic Press, 173–265.

——, and M. J. Suarez, 1983: Vertical differencing of the primitive equations in sigma coordinates. *Mon. Wea. Rev.*, **111,** 34–45.

——, and S. Moorthi, 1988: Baroclinic instability in vertically discrete systems. *J. Atmos. Sci.*, **45,** 1688–1707.

——, and Y.-J. G. Hsu, 1990: Energy conserving and potential-enstrophy dissipating schemes for the shallow water equations. *Mon. Wea. Rev.*, **118,** 1960–1969.

——, and C. S. Konor, 1994: A generalized vertical coordinate and the choice of vertical grid for atmospheric models. *Life Cycles of Extratropical Cyclones*, Vol. III, Bergen, Norway, University of Norway, 259–264.

——, and ——, 1996: Vertical differencing of the primitive equations based on the Charney–Phillips grid in hybrid σ–θ vertical coordinates. *Mon. Wea. Rev.*, **124,** 511–528.

——, C. R. Mechoso, and C. S. Konor, 1992: An isentropic vertical coordinate model: Design and application to atmospheric frontogenesis studies. *Meteor. Atmos. Phys.*, **50,** 31–45.

——, C. S. Konor, and C. R. Mechoso, 1994: A generalized vertical coordinate and the choice of vertical grid for atmospheric models. Preprints, *10th Conf. on Numerical Weather Prediction*, Portland, OR, Amer. Meteor. Soc., 32–34.

Black, T. L., 1984: Numerical experiments of jet streak ageostrophic circulations using pseudogeostrophic initialization and perspectives. Ph.D. dissertation, University of Wisconsin—Madison, 185 pp. [Available from University of Wisconsin—Madison, Space Science and Engineering Center, Madison, WI 53706.]

Bleck, R., 1973: Numerical forecasting experiments based on the conservation of potential vorticity on isentropic surfaces. *J. Appl. Meteor.*, **12,** 737–752.

——, 1977: Numerical simulation of Lee cyclogenesis in gulf of Genoa. *Mon. Wea. Rev.*, **105,** 428–445.

——, 1978a: On the use of hybrid vertical coordinates in numerical weather prediction models. *Mon. Wea. Rev.,* **106,** 1233–1244.
——, 1978b: Finite difference equations in generalized vertical coordinates. Part I: Total energy conservation. *Beitr. Phys. Atmos.,* **51,** 360–372.
——, 1979: Finite difference equations in generalized vertical coordinates. Part II: Potential vorticity conservation. *Beitr. Phys. Atmos.,* **52,** 95–105.
——, 1984: An isentropic coordinate model suitable for lee cyclogenesis simulation. *Riv. Meteorol. Aeronaut.,* **43,** 189–194.
——, and S. Benjamin, 1993: Regional weather prediction with a model combining terrain-following and isentropic coordinates. Part I. *Mon. Wea. Rev.,* **121,** 1770–1785.
Charney, J. G., and N. A. Phillips, 1953: Numerical integration of the quasigeostrophic equations for barotropic and simple baroclinic flows. *J. Meteor.,* **10,** 71–99.
Cullen, M. J. P., and J. James, 1994: A comparison of two different vertical grid staggerings. Preprints, *10th Conf. on Numerical Weather Prediction,* Portland, OR, Amer. Meteor. Soc., 38–40.
Deaven, D. G., 1976: A solution on boundary problems in isentropic coordinate models. *J. Atmos. Sci.,* **33,** 1702–1713.
Eliassen, A., and A. Raustein, 1968: A numerical integration experiment with a model atmosphere based on isentropic surfaces. *Meteor. Ann.,* **5,** 45–63.
——, and ——, 1970: A numerical integration experiment with a six-level atmospheric model with isentropic information surface. *Meteor. Ann.,* **5,** 429–449.
Friend, A. L., D. Djuric, and K. C. Brundidge, 1977: A combination of isentropic and sigma coordinates in numerical weather prediction. *Beitr. Phys. Atmos.,* **50,** 290–295.
Gall, R. L., and D. R. Johnson, 1977: Prediction of a quasi-steady propagating jet core with an isentropic numerical model. Isentropic Numerical Models: Results on Model Development for Zonally Averaged and Secondary Circulations, Rep. to NSF, Dept. of Meteor. and Space Sci. and Engineering Center, University of Wisconsin—Madison, 1–88. [NTIS PB283480/AS.]
Hollingsworth, A., 1995: A spurious mode in the ''Lorenz'' arrangement of Φ and T which does not exist in the ''Charney–Phillips'' arrangement. ECMWF Tech. Memo. 211, 12 pp. [Available from ECMWF, Shinfield Park, Reading RG2 9AX, United Kingdom.]
Hoskins, B. J., M. E. McIntyre, and A. W. Robertson, 1985: On the use and significance of isentropic potential vorticity maps. *Quart. J. Roy. Meteor. Soc.,* **111,** 877–946.
Hsu, Y.-J. G., and A. Arakawa, 1990: Numerical modeling of the atmosphere with an isentropic vertical coordinate. *Mon. Wea. Rev.,* **118,** 1933–1959.
Johnson, R. D., and L. W. Uccellini, 1983: A comparison of methods for computing the sigma-coordinate pressure gradient force for flow over sloped terrain in a hybrid theta–sigma model. *Mon. Wea. Rev.,* **111,** 870–886.
——, T. H. Zapotocny, F. M. Reames, B. J. Wolf, and R. B. Pierce, 1993: A comparison of simulated precipitation by hybrid isentropic–sigma and sigma models. *Mon. Wea. Rev.,* **121,** 2088–2114.
Konor, C. S., C. R. Mechoso, and A. Arakawa, 1994: Comparison of frontogenesis simulations with θ and σ vertical coordinates and design of a general vertical coordinate model. *Life Cycles of Extratropical Cyclones,* Vol. II, Bergen, Norway, University of Bergen, 464–468.
Lorenz, E. N., 1960: Energy and numerical weather prediction. *Tellus,* **12,** 364–373.
Mesinger, F., and A. Arakawa, 1976: Numerical methods used in atmospheric models. GARP Publication Series 17, Part I, 64 pp.
Phillips, N. A., 1957: A coordinate system having some special advantages for numerical forecasting. *J. Meteor.,* **14,** 184–185.
——, 1974: Application of Arakawa's energy-conserving layer model to operational weather prediction. National Meteorological Center, NWS/NOAA Office Note 104, 40 pp.
Shapiro, M. A., 1974: The use of isentropic coordinates in the formation of objective analysis and numerical prediction models. *Atmosphere,* **12,** 10–17.
——, 1975: Simulation of upper-level frontogenesis with a 20-level isentropic coordinate primitive equation model. *Mon. Wea. Rev.,* **103,** 591–604.
Simmons, A. J., and M. Burridge, 1981: An energy and angular-momentum conserving vertical finite-difference scheme and hybrid vertical coordinates. *Mon. Wea. Rev.,* **109,** 758–766.
Uccellini, L. W., D. R. Johnson, and R. E. Schlesinger, 1979: An isentropic and sigma coordinate hybrid numerical model: Model development and some initial tests. *J. Atmos. Sci.,* **36,** 390–414.
Zapotocny, T. H., D. R. Johnson, and F. M. Reames, 1994: Development and initial test of the University of Wisconsin global isentropic–sigma model. *Mon. Wea. Rev.,* **122,** 2160–2178.
Zhu, Z., J. Thuburn, B. J. Hoskins, and P. H. Haynes, 1992: A vertical finite-difference scheme based on a hybrid σ–θ–p coordinate. *Mon. Wea. Rev.,* **120,** 851–862.